

1  
2 **Combined loading capacity of skirted circular foundations in**  
3 **loose sand**

4  
5 Manuscript submitted to Ocean Engineering on 17 April 2018; accepted 28 April 2019.

6  
7 **Nicole Fiumana (corresponding author) \***  
8 PhD candidate  
9 Email: [nicole.fiumana@research.uwa.edu.au](mailto:nicole.fiumana@research.uwa.edu.au)

10  
11 **Britta Bienen \***  
12 Associate Professor  
13 Email: [britta.bienen@uwa.edu.au](mailto:britta.bienen@uwa.edu.au)

14  
15 **Laura Govoni +**  
16 Researcher  
17 Email: [l.govoni@unibo.it](mailto:l.govoni@unibo.it)

18  
19 **Susan Gourvenec \* (^)**  
20 Professor  
21 Email: [susan.Gourvenec@southampton.ac.uk](mailto:susan.Gourvenec@southampton.ac.uk)

22  
23 **Mark J. Cassidy \* (#)**  
24 Professor  
25 Email: [mark.cassidy@unimelb.edu.au](mailto:mark.cassidy@unimelb.edu.au)

26  
27 **Guido Gottardi+**  
28 Professor  
29 Email: [guido.gottardi2@unibo.it](mailto:guido.gottardi2@unibo.it)

30  
31 \*Centre for Offshore Foundation Systems and ARC CoE for Geotechnical Science and  
32 Engineering  
33 The University of Western Australia  
34 35 Stirling Hwy  
35 Crawley, Perth, WA 6009  
36 Australia  
37 Fax: +61 (0) 8 6488 1044

38  
39 + DICAM  
40 University of Bologna  
41 Viale Risorgimento, 2  
42 40125, Bologna  
43 Italy

44  
45 Formerly \*, now ^ Faculty of Engineering and Physical Sciences  
46 University of Southampton, UK  
47 +44 (0)23 80599139

48 Formerly \*, now # Melbourne School of Engineering  
49 The University of Melbourne  
50 +61 383446619  
51  
52 No. of words: 4554 (excluding abstract, references and figures)  
53 No. of tables: 5  
54 No. of figures: 14  
55  
56  
57

58 **Abstract**

59 Skirted foundations are an attractive foundation concept in the offshore energy sector,  
60 both for wind turbines and oil and gas platforms. Most of the evidence of skirted  
61 foundation behaviour under combined vertical, horizontal and moment (VHM) loading  
62 in sand has been collected from small-scale model experiments conducted at unit gravity  
63 on the laboratory floor. This paper presents results from a series of centrifuge experiments  
64 of skirted foundations on loose silica sand at relevant prototype stress levels. The vertical  
65 load-penetration curve is shown to be predicted well using established analytical methods.  
66 Centrifuge modelling results provide experimental evidence of the complex effects of the  
67 interaction of skirt aspect ratio and relative stress level on the VHM yield surface. A  
68 conservative and design-oriented solution based on the yield envelope approach describes  
69 available foundation capacity within the established framework of strain-hardening  
70 plasticity theory.

71 **Key words:** Skirted foundation; capacity; combined loading; centrifuge modelling; sand.

72

## 73 INTRODUCTION

74 Skirted foundations find wide application offshore for both fossil and renewable energy  
75 installations. Traditionally employed in fine grained seabeds for oil and gas facilities  
76 (Christoffersen 1993), their use has been extended to jacket supported structures in sandy  
77 seabeds (Bye et al. 1995). Shallowly embedded skirted foundations offer a convenient  
78 solution as foundations for jack-up units, either as an alternative or in combination with  
79 spudcan foundations (e.g. Vlahos et al. 2006; Bienen et al. 2012; Vulpe et al. 2013; Cheng  
80 & Cassidy 2016). Skirted foundations have been also considered as a cost-effective  
81 alternative to monopiles in supporting wind turbines (e.g. Borkum Riffgrund 1 in the  
82 North Sea and 71 Aberdeen Offshore Wind Farm off the east coast of Scotland), in the  
83 form of suction caissons either as a monopod or in a group of three or four foundations  
84 of a jacket (e.g. Byrne & Houlsby 2002; Houlsby, et al., 2005; Houlsby 2016; Tjelta  
85 2015). Different uses of skirted foundations in the offshore environment are shown  
86 schematically in Figure 1. Figure 1a and Figure 1b depict a monopod and jacket  
87 arrangement for wind turbines while Figure 1c and Figure 1d illustrate a jack-up unit and  
88 jacket structure, respectively. Skirted foundations can vary in diameter from about 6 m to  
89 8 m for a jacket supported offshore wind turbine to a range of 10 m to 20 m for oil and  
90 gas jackets, monopod supported offshore wind turbines and jack-ups. The aspect ratio of  
91 the skirt length  $d$  to diameter  $D$  is generally less than 1 m in sand, with  $d/D$  of 0.25 or less  
92 required in jack-ups to ensure the skirts can be lifted back inside the holding for  
93 redeployment.

94 Significant horizontal load ( $H$ ) and overturning moment ( $M$ ) characterise load paths of  
95 offshore foundations. In general, actions on skirted foundations for wind turbines are  
96 characterised by low values of vertical load ( $V$ ), compared to those of oil and gas  
97 platforms. Bearing pressures  $V/A$ , where  $A$  is the plan area of the foundation, generally  
98 range between 40 to 125 kPa (Byrne et al. 2002; Houlsby & Byrne 2005) in offshore wind  
99 applications, and 300 to 760 kPa (Cassidy et al. 2004; Bienen et al. 2009) in oil and gas  
100 installations. The capacity of foundations to withstand combined vertical ( $V$ ), horizontal  
101 ( $H$ ) and moment ( $M$ ) loading can be conveniently expressed in terms of a yield surface.

102 Early investigations of the yield surface of foundations in sand were based on data of  
103 single gravity experiments on small flat plates in dense (Gottardi et al. 1999) and loose

104 sand (Nova & Montrasio 1991; Gottardi & Butterfield 1995; Bienen et al. 2006; Bienen  
105 et al. 2007). These studies made extensive use of the swipe testing procedure that was  
106 first used by Tan (1990) to track a path along the yield surface in a single experiment.  
107 The test results consistently suggested that the yield surface of a shallow foundation  
108 expands with mobilised vertical load ( $V_0$ ), which can be uniquely described in normalised  
109 load space (normalising the load axes by  $V_0$ ) by the following equation (Gottardi et al.  
110 1999)

$$\left(\frac{M/D}{m_0 V_0}\right)^2 + \left(\frac{H}{h_0 V_0}\right)^2 - 2\alpha \frac{HM/D}{m_0 h_0 V_0^2} - \beta_{12}^2 \left(\frac{V}{V_0}\right)^{2\beta_1} \left(1 - \frac{V}{V_0}\right)^{2\beta_2} = 0 \quad \text{Eq. 1}$$

111 where  $\beta_1$  and  $\beta_2$  are shape parameters influencing where the peak horizontal and moment  
112 loads occur under vertical load, and  $\beta_{12} = \frac{(\beta_1 + \beta_2)^{(\beta_1 + \beta_2)}}{\beta_1^{\beta_1} \beta_2^{\beta_2}}$ . The coefficients  $m_0$  and  $h_0$   
113 control the size of the yield surface in the moment and horizontal load plane respectively.

114 Eq. 1 has been shown to accurately represent the yield surface of shallow surface  
115 foundations at prototype stress conditions, as demonstrated through a series of centrifuge  
116 swipe tests on flat plates on medium dense sand (Cassidy 2007; Govoni et al. 2010; Cheng  
117 & Cassidy 2016) and tests of a full jack-up platform with three conical spudcan  
118 foundations on dense sand (Bienen et al. 2009).

119 The effect of the skirt length on the yield surface in drained conditions on sand was first  
120 addressed with reference to bucket foundations of different embedment ratios (skirt  
121 length  $d$  to diameter  $D$ ) ( $d/D = 0, 0.166, 0.33, 0.66$ ) on very dense sand samples (Byrne  
122 & Houlsby 1999; Byrne 2000). Single gravity tests, mostly of the swipe type, were carried  
123 out at low values of vertical load  $V_0 \leq 0.25 \leq V_{\text{peak}}$ , where  $V_{\text{peak}}$  identifies the value of the  
124 peak vertical bearing capacity, with results showing that the normalised yield surface  
125 increases (i.e.  $h_0$  and  $m_0$  become larger) with decreasing  $V_0/V_{\text{peak}}$ . At low vertical load the  
126 response deviates from the parabolic yield surface shape to follow a frictional sliding  
127 surface, dilatant in the presence of dominant overturning moment ( $M$ ) and contractant  
128 when the horizontal component of the load ( $H$ ) is dominant. This concept of the yield  
129 surface is illustrated in Figure 2a, in planes containing the vertical load ( $V$ ) axis. A similar  
130 dependency of the normalised yield surface shape and size on the load path was also  
131 exhibited by spudcan foundations subjected to swipe tests on sand in the centrifuge

132 (Cheng 2015; Cheng & Cassidy 2016a). Results of centrifuge swipe tests on flat plates  
133 buried in medium dense sand samples also displayed a similar pattern, which included a  
134 high non-vertical load capacity at low and even negative values of the vertical load  
135 (Govoni et al. 2011). Non-zero horizontal and moment capacity in the tensile range of the  
136 vertical load was also shown in results of skirted foundation model tests under combined  
137 loading on loose sand at 1g (Villalobos 2006). In order to accommodate the  
138 experimentally observed behaviour, Villalobos et al. (2009) expressed the yield surface  
139 as follows and as qualitatively represented in Figure 2b.

$$\left(\frac{M/D}{m_0 V_0}\right)^2 + \left(\frac{H}{h_0 V_0}\right)^2 - 2\alpha \frac{HM/D}{m_0 h_n V_0^2} - \beta_{12}^2 \left(\frac{V}{V_0} + t_0\right)^{2\beta_1} \left(1 - \frac{V}{V_0}\right)^{2\beta_2} = 0 \quad \text{Eq. 2}$$

140 where  $t_0$  is defined as the yield surface tension parameter.

141 A similar expression for the yield surface was recently used to interpret the combined  
142 loading response of a skirted foundation on dense sand based on evidence from 1g  
143 experiments (Foglia et al. 2015).

144 A summary of the experimental research on the VHM yield surface of shallow  
145 foundations on sand is given in Table 1.

146 Though these studies have shown that foundation embedment has a marked influence on  
147 the VHM yield surface, particularly at low values of vertical load mobilisation ( $V_0$ ),  
148 evidence at prototype stress levels is lacking. This study therefore aims to close the gap  
149 in providing centrifuge experimental evidence of the VHM yield surface of circular  
150 skirted foundations in sand investigating the effect of two different skirt aspect ratios ( $d/D$   
151 = 0.25 and  $d/D = 0.5$ ) on the horizontal and moment capacity. Both high and low stress  
152 levels reflective of the prototype are considered. The specific contributions of this paper  
153 are:

- 154 • new experimental evidence on the vertical and combined planar VHM loading  
155 response of skirted foundations on sand at stress levels reflective of the prototype;
- 156 • insights into the effects of skirt aspect ratio ( $d/D$ ) and stress level on the horizontal and  
157 moment capacity;

- 158 • recommendations for the assessment of VHM capacity of skirted foundations in sand  
159 in practice.

160

161

## 162 **EXPERIMENTAL SET-UP AND PROCEDURE**

### 163 **Drum centrifuge, VHM actuator and model foundation**

164 The experiments were carried out in the 1.2 m diameter drum centrifuge at the University  
165 of Western Australia (Stewart et al. 1998). The soil model is contained in the drum  
166 channel, which is 0.3 m wide and 0.2 m deep. Two concentric shafts allow independent  
167 control of the drum and testing instruments connected to the central actuator.

168 An in-house developed VHM apparatus (Zhang et al. 2013) was used in the experiments.  
169 The vertical, horizontal and rotational foundation displacements are applied by movement  
170 of two actuators, which are linked as shown in Figure 3. The movement is transferred to  
171 the foundation via an instrumented tubular section, which is strain-gauged to measure  
172 vertical as well as moment loading in two locations. This allows the vertical, horizontal  
173 and moment load at a reference point (RP) on the foundation to be determined, assuming  
174 linear variation of the bending moment. Any combination of vertical, horizontal and  
175 rotational movement (as defined in Figure 3) of the foundation reference point (within  
176 the scope of the VHM actuator) can be prescribed to be independently controlled, with a  
177 rotational component requiring simultaneous compensations in vertical and horizontal  
178 movements (Figure 4). Further details on the apparatus can be also found in Cheng and  
179 Cassidy (2016).

180 Two foundation models, fabricated from aluminum, were used in the experiments. The  
181 foundation diameter  $D$  was 50 mm in both models, representing a prototype diameter of  
182 5 m when tested at 100 g. One model featured a skirt length  $d$  of 12.5 mm, resulting in an  
183 aspect ratio  $d/D = 0.25$ , the other had a skirt length of 25 mm giving an aspect ratio  $d/D$   
184  $= 0.5$ . The skirt thickness  $t$  was 1 mm, selected to ensure sufficient robustness to ensure  
185 against buckling during installation and combined load testing. The models (shown in  
186 Figure 3) were provided with an electronic venting system chosen to enable in-flight  
187 installation and sealing. The seal was remotely actuated once the lid came in contact with

188 the soil. The venting system ensured no water was trapped inside the skirt compartment  
189 of the penetrating foundation and hence no significant excess pore pressure could occur  
190 during installation within the plug.

191

## 192 **Soil sample**

193 The experiments were performed in commercially available silica sand, which is routinely  
194 used at UWA. Table 2 summarises the sand properties (Liu & Lehane 2012). The sample  
195 was prepared by pluviation through 165 mm of water while the centrifuge was spinning  
196 at 20g. Once the raining process was complete, the water was drained out of the channel,  
197 the centrifuge was stopped and a plastic scraper was used to level the surface. The final  
198 sand sample height was 150 mm. The sample was resaturated in flight over night prior to  
199 testing.

200 The sample preparation procedure produced a loose soil sample, characterised through  
201 miniature cone penetrometer tests (CPT) with a cone diameter of 6 mm. Tests were  
202 carried out at various locations around the sample. The penetration rate of the cone was  
203 0.1 mm/s. Noting the water saturation of the sand sample in the centrifuge, the response  
204 is expected to be drained. The criterion  $V = vD/cv$  is typically employed to estimate the  
205 drainage response. With values relevant to this series of tests,  $V = 4e-4 < 0.01$ , below  
206 which the response is expected to be drained (Jaeger et al. 2010). Figure 5 shows a  
207 representative CPT result in terms of cone tip resistance  $q_c$  and dimensionless net tip  
208 resistance  $q_{net}$  with penetration  $w$  and normalised penetration  $w/D$ , respectively, where  $D$   
209 is the diameter of the skirted foundation.

$$q_{net} = (q_c - \sigma_{v0})/\sigma'_{v0} \quad \text{Eq. 3}$$

210 An average relative density  $D_r$  of 30% was derived from the experimental results  
211 according to the relationship (Schneider & Lehane, 2006).

$$D_r = 100(q_{net}/250)^{0.5} \quad \text{Eq. 4}$$

212 The effective unit weight was computed from mass measurements of the sample and  
213 returning a value of  $\gamma' = 10 \text{ kN/m}^3$ .



214

215 **Experimental strategy and testing program**

216 The experimental program comprised a series of vertical penetration and swipe tests.  
217 Vertical penetration tests were carried out with and without unload-reload cycles on both  
218 foundation models to obtain the evolution of uniaxial capacity with foundation  
219 penetration and an indication of vertical unloading stiffness. The vertical load-penetration  
220 tests allowed selection of the target penetration depths at which swipe tests were  
221 performed.

222 Swipe tests formed the majority of events included in this centrifuge testing program.

223 In order for the centrifuge tests to reflect prototype behaviour, both foundation penetration  
224 and swipe tests need to be performed at enhanced gravity. The footing was installed at  
225 100g with the vent open. When the lid invert came into contact with the soil surface, the  
226 valve was closed. The entire procedure was executed without stopping the centrifuge. In  
227 swipe tests, the foundation was further penetrated to the target vertical displacement ( $w_0$ ).  
228 The vertical load mobilised at this point is termed  $V_0$ . The vertical displacement was then  
229 held constant while horizontal displacement ( $u$ ), rotation ( $\theta$ ) or a constant combination of  
230 the normalised ratio  $u/D\theta$  were applied to the foundation RP. The swipe tests commenced  
231 immediately after reaching the target penetration, so that there were no delays causing  
232 relaxation and leading to the load paths lying inside, rather than tracking the VHM yield  
233 surface (Bienen et al. 2007). The RP was located at the underside of the foundation base  
234 plate (Figure 3), similar to previous experiments under drained conditions (e.g. Villalobos  
235 2006). The tests were performed entirely under displacement control at a model rate of  
236 0.1mm/s in all directions so as a drained soil response was ensured (Cheng & Cassidy  
237 2016b). All swipe tests commenced from  $V_0$ , without unloading.

238 Two values of vertical penetration were targeted in the experiments ( $w_0 = 0.6D$ ;  $0.3D$ ,  
239 Table 3), corresponding to low and high values of vertical bearing pressure  $V/A$  of 100  
240 kPa and 500 kPa, respectively. These bearing pressures are relevant to the offshore energy  
241 installations shown in Figure 1. For each target stress level and skirt length of the  
242 foundation model, four different displacement ratios  $u/D\theta$  were investigated in order to

243 obtain sufficient evidence of the VHM yield surface in three-dimensional space. The  
244 experimental program included 16 swipe tests, which are summarized in Table 3.

245

246

## 247 **RESULTS AND DISCUSSION**

### 248 **Presentation of results and notation**

249 The experimental results are presented in prototype dimensions  $V$ ,  $H$ ,  $M$ ,  $w$ ,  $u$ ,  $D\theta$ ,  
250 respectively for load and displacements, and normalised quantities to allow comparisons.

251 The normalisation for the vertical displacements is  $w/D$ , while for the load components a  
252 selection of normalisations are adopted, according to the stress level  $V/A$ ,  $V/A\gamma'(d+D/2)$ ,  
253  $V/\pi\gamma'(D^3/8)$  and to the reference load for the interpretation of the swipe tests,  $V/V_0$ ,  $H/V_0$ ,  
254  $M/DV_0$ .

255

### 256 **Vertical load-penetration curve**

257 The vertical load-penetration curves are presented in Figure 6a, including the dedicated  
258 tests with and without unload-reload loops on both foundation models as well as the initial  
259 vertical loading phase of all swipe tests. The results also serve to confirm uniformity of  
260 the soil sample, as the data for each of the two foundation models are tightly grouped.

261 The penetration resistance increases approximately linearly initially as the skirts penetrate  
262 the sand. The gradient of the penetration resistance changes markedly as the lid invert  
263 comes into contact with the soil. At this point the bearing pressure  $V/A$  is approximately  
264 100 kPa for the foundation with the aspect ratio  $d/D = 0.25$  and 245 kPa for  $d/D = 0.5$ .

265 The obtained load-displacement relationship demonstrates the characteristic response of  
266 foundation penetration in loose sand, with bearing capacity increasing monotonically  
267 with penetration. The target penetration depths selected to achieve the desired stress levels  
268 at the commencement of the swipe tests are indicated in Figure 6a.

269 Normalisation of the bearing pressure by the soil self-weight stress level half a diameter  
270 below the skirt tip as proposed in Govoni et al. 2011, unifies the measured response of  
271 the two aspect ratios as shown in Figure 6b.

272 The observed response during skirt penetration is well predicted using the bearing  
273 capacity based approach outlined in Houlsby and Byrne (2005) as the sum of the friction  
274 developing in the inner (i) and outer (o) part of the skirt and the bearing resistance of the  
275 skirt annulus (Eq. 5). The linear prediction is plotted in terms of normalised quantities in  
276 Figure 6b with reference to the foundation with a ratio  $d/D = 0.25$ .

$$V = \frac{\gamma' w^2}{2} (K \tan \delta)_o (\pi D_o) + \frac{\gamma' w^2}{2} (K \tan \delta)_i (\pi D_i) + \left( \gamma' w N_q + \gamma' \frac{t}{2} N_\gamma \right) (\pi A_{\text{tip}}) \quad \text{Eq. 5}$$

277 Villalobos (2006) suggests the use of the Rankine passive coefficient  $K = (1 + \sin \phi) / (1 -$   
278  $\sin \phi)$  to be a good approximation for the analysis of the skirt penetration for the case of a  
279 smooth skirt. The drained bearing capacity factors were computed with the software ABC  
280 (Martin 2003) for a surface strip foundation (Villalobos 2006) of breadth  $B = D$  resting  
281 on sand ( $\gamma' = 10 \text{ kN/m}^3$  and  $\phi = 31^\circ$ ) and equal to  $N_q = 20.90$  and  $N_\gamma = 17.95$ . The frictional  
282 properties considered for the sand refer to a friction angle,  $\phi = 31^\circ$  and an interface friction  
283 angle between the soil and the skirt wall,  $\delta = 2/3 \phi = 21^\circ$ . In the present study, the  
284 enhancement of stress due to the frictional forces close to the skirt wall was not taken into  
285 account, which would instead represent a more conservative solution (Houlsby & Byrne  
286 2005). However, Figure 6 shows the prediction using Eq. 5 to be consistent with the  
287 experimental results.

288 Alternatively, the model proposed by Andersen et al. 2008 also provides a good  
289 estimation of the skirt penetration behaviour, which uses a smaller  $K$  value, but includes  
290 the effect of the additional stress on the tip resistance. The parameters  $N_q$  and  $N_\gamma$  were  
291 selected equal to 74 and 95 respectively as related to field model tests more similar to the  
292 herein prototype (Andersen et al. 2008) and  $K=0.8$  (Figure 6b). Details on the equation  
293 can be found in Andersen et al. 2008.

294 Figure 6b also reports the drained bearing capacity prediction from the software ABC  
295 (Martin 2003), considering a smooth circular foundation of 5 m diameter on a soil with  
296  $\gamma' = 9.94 \text{ kN/m}^3$  and  $\phi' = 31^\circ$ . The penetration was simulated by computing the bearing  
297 pressure for increasing values of overburden pressure  $q$ . The touchdown value and the  
298 non-linearity of the behaviour during penetration result was slightly overestimated (20%)  
299 with respect to the experimental data. This could be due to the assumption of an associated

300 flow in the limit analysis program which is known to lead to over-prediction of vertical  
301 bearing capacity in sand. Another possibility is the gradual mobilisation of resistance in  
302 the physical experiment, which is in contrast with the instantaneous full resistance  
303 modelled numerically. This method, however, provides a closer reproduction of the  
304 response with respect to buried footings or spudcan hardening laws (Govoni et al. 2011;  
305 Cheng & Cassidy 2016).

306 The hardening laws for buried (Govoni et al. 2011) and spudcan foundations (Cheng &  
307 Cassidy 2016a) are included in Figure 6b for comparison. The adopted relationship to  
308 describe the pure plastic response of the skirted foundations under monotonic vertical  
309 loads was that proposed by Bienen et al. (2006) and rewritten in terms of dimensionless  
310 parameters (Govoni et al. 2011):

$$\frac{V}{(A\sigma'_v)} = \left(\frac{DK_1}{A\sigma'_v}\right) \frac{w_p}{D} \left[ \frac{1 + \frac{w_p}{D} \left(\frac{D}{w_1}\right)}{1 + \frac{w_p}{D} \left(\frac{D}{w_2}\right)} \right] \quad \text{Eq. 6}$$

311 where the best fit coefficients are:  $(DK_1)/(A\sigma'_v) = 19417.6$ ,  $w_1/D = -1.16$ ,  $w_2/D =$   
312  $2.23$  and where  $(DK_1)/(A\sigma'_v)$  represents the dimensionless stiffness, with  $\sigma'_v = \gamma'(d +$   
313  $D/2)$  (Bolton & Lau 1988).

314 Incorporation of unload-reload loops into vertical load-penetration tests provide an  
315 indication of the elastic stiffness of the soil-foundation system. Obtained values are  
316 plotted in Figure 7 against the related stress level. The normalised form  $Dk_e/A\sigma'_v$  allows  
317 comparison with obtained values for a spudcan foundation on loose sand (Cheng &  
318 Cassidy 2016a) and buried foundations on medium dense sand (Govoni et al. 2011),  
319 showing a good agreement.

320 The unload stiffness can be also compared with theoretical solutions, for instance  $K_v =$   
321  $\frac{V}{w_{GR}}$  (Doherty & Deeks 2003). By assuming a representative shear modulus for the soil  
322  $G = 13.8 \text{ N/mm}^2$  (Cheng & Cassidy 2016b), an average normalised stiffness  $Dk_e/A\sigma'_v =$   
323  $1513$  was obtained (Figure 7).

324 A value for the elastic stiffness of  $Dk_e/(A\sigma'_{v0}) = 1266$  was used to plot the derived  
325 relationship for the plastic response (Eq. 6) in terms of total displacements. From the  
326 comparison with the hardening laws derived for a spudcan (Cheng & Cassidy 2016a) and  
327 a buried foundation (Govoni et al. 2011) in Figure 6b, the response appears to be  
328 qualitatively similar. The scatter deriving from geometrical effects and higher density of  
329 the sample of the buried foundations (Figure 6), suggests neither equation is suitable for  
330 the description of the vertical penetration of skirted foundations.

331 Figure 8 compares the installation response obtained from 1g vertical penetration tests  
332 with those from the centrifuge test data of this study. The 1g data refer to the work of  
333 Villalobos (2006), and details of the test characteristics are provided in Table 4 in terms  
334 of  $d/D$  ratio, relative density of the sample, vertical load and displacement measured at  
335 full contact of the foundation lid with the soil. The comparison is presented first as bearing  
336 pressure – normalised displacement response (Figure 8a), which highlights the low  
337 stresses in the 1g tests, and secondly in the load normalisation proposed by Bolton and  
338 Lau (1989) (Figure 8b), with the specific purpose of comparing 1g and centrifuge tests.  
339 However, as the effect of stress level on the stiffness is not captured by this normalisation,  
340 it fails to unify the measured responses. This confirms the observations reported in Bienen  
341 et al. (2007) with a very stiff initial load-displacement response and enhanced mobilised  
342 friction angle due to increased dilatancy at the low stress levels at 1g and reinforces the  
343 importance of the stress state of the soil on foundation behaviour.

344

### 345 **Capacity under combined VHM loading**

346 In this section, the observed response during swipe tests dominated by moment and  
347 horizontal load, respectively, is discussed. Results of all swipe tests are then presented,  
348 with discussion of the effects of the level of vertical load and foundation aspect ratio on  
349 the VHM yield surface. The analysis is then discussed in terms of deviatoric components,  
350 before expressions to fit the foundation capacity are explored.

351

#### 352 *Response under predominantly horizontal or moment loading*

353 Figure 9 shows results obtained for the four tests (combinations of  $d/D = 0.25, 0.5$ ;  $V/A$   
354  $= 100, 500$  kPa) executed with a displacement ratio  $u/D\theta = -0.1$ , resulting in a response

355 dominated by moment. The response is in accordance with typical swipe results, with the  
356 vertical reaction decreasing as moment load increases, tracing a parabolic shape in the  
357 dominant VM plane. The horizontal load continues to increase, at low levels, in all tests  
358 following an initial minimum (Figure 9a), and all tests exhibit a peak in moment capacity  
359 (Figure 9a and c). The tests of both foundation aspect ratios commencing from low  $V_0$   
360 ( $\sim 100\text{kPa}$ ) values exhibit strongly dilatant behaviour when the load paths leave the  
361 parabolic section of the yield surface (Figure 9b and d), but this is suppressed at high  
362 initial bearing pressure ( $\sim 500\text{kPa}$ ). In the case of a low foundation aspect ratio ( $d/D =$   
363  $0.25$ ) and high  $V_0$ , the peak moment is only marginally higher than the moment loading  
364 maintained for the remainder of the test (Figure 9a). The test with foundation of higher  
365 aspect ratio ( $d/D = 0.5$ ), also at high  $V_0$ , results in slightly contractant behaviour in the V-  
366 M/D plane (Figure 9d). Similar observations were reported on the basis of 1g tests of  
367 skirted foundations on dense sand at low stress levels (Byrne 2000) and more recent  
368 centrifuge tests of spudcan foundations (Cheng & Cassidy 2016a).

369 Figure 10 shows results obtained for a group of tests executed with a displacement ratio  
370  $u/(D\theta) = \infty$ , for which the horizontal load dominates the response. A similar observation  
371 to the previous example of a parabolic trace of the yield surface in the dominant loading  
372 plane (VH) is observed. Tests performed at high  $V_0$  show a marked peak in the horizontal  
373 reaction, (with reference to prototype units), and appears more evident for the smaller  
374 aspect ratio (Figure 10a and c). A dilatant behaviour is evident in the test at low  $V_0$  and  
375  $d/D = 0.5$  (Figure 10d), reached when the vertical reaction becomes negative. For low  $V_0$   
376 and small aspect ratio (Figure 10a) the test reaches a ‘parallel point’ (Tan 1990), after  
377 which the reactions remain constant despite increasing displacements. A parallel point is  
378 also observed for tests SW3, SW9 and SW11, performed at high  $V_0$  (Figure 9a and 9c,  
379 Figure 10c).

380

### 381 *All experimental results in the VH and VM planes*

382 The obtained load response of all the swipe tests is presented in four pairs of plots,  
383 organised by the displacement ratio applied in the swipe event. These are presented in  
384 terms of prototype units in Figure 11 and normalised quantities in Figure 12.

385 The experimental results initially trace a parabolic yield surface before the load paths  
386 proceed along a sliding surface, with low stresses generally resulting in dilatant response.  
387 At higher stresses, the behaviour tends towards a parallel point. For the swipe  
388 displacement ratio  $u/D\theta = 1.15$  dilatant behaviour resulted independent of skirt aspect  
389 ratio and stress level, which is in contrast to tests subjected to horizontal displacement  
390 and rotation in opposing directions.

391 Figure 11 allows a better visual understanding of the effect of the skirt length on the  
392 capacity. Byrne (2000) observed that an increase in the skirt length leads to an increase  
393 in the yield surface only in the horizontal direction. This behaviour appears here more  
394 pronounced for swipe tests performed at low  $V_0$ .

395 The normalised load paths presented in Figure 12 further illustrate the common general  
396 trend in the shape of the yield surface, with some differences arising from the stress level  
397 and skirt length, depending on the load path. The centrifuge experimental evidence  
398 supports the concept of a family of yield surfaces, with elements of the expressions  
399 proposed by Byrne and Houlsby (999) and Villalobos et al. (2009) present (Figure 2). For  
400 the first two sets of displacement ratios ( $u/D\theta = \infty$  and  $u/D\theta = -1.15$ ) the swipe events  
401 terminate at  $V/V_0 \leq 0$  in combination with non-zero values of horizontal or moment loads.  
402 This is not evident for flat foundations (Govoni et al. 2011) and suggests the foundation  
403 skirts enhance the yield surface to encapsulate also tensile loads. However, this does not  
404 seem to hold for the other displacement ratios and hence should not be relied on in the  
405 overall performance of the foundation.

406

407 *All experimental results in the HM plane*

408 Figure 13 compares the experimental results in the M/D vs H plane for a)  $d/D = 0.25$  and  
409 b)  $d/D = 0.5$ . The data are presented in prototype units.

410 The load paths obtained by imposing the fixed displacement ratios on the swipe tests  
411 extend over two quadrants for all the tests. Displacement ratios  $u/D\theta = \infty$  and  $u/D\theta =$   
412  $-1.15$  present positive values of horizontal reaction, H, while the moment load  
413 component, M/D, starts negative, decreases to zero, and assumes positive values at the

414 end of the swipe event. The tests dominated by moment ( $u/D\theta = -0.1$ ) in a similar way  
415 feature an initial negative horizontal reaction, ending with positive values.

416 The resulting load paths are quite complex, with a variable ratio of horizontal and moment  
417 loads developing during the swipe event, for constant displacement ratios applied. Swipe  
418 tests, in which similar displacement ratios were applied, display similar load paths  
419 initially, differing later depending on the level of vertical load applied. Greater skirt length  
420 ( $d/D = 0.5$ ) leads to wider coverage of the load space, and later divergence of load paths  
421 depending on the vertical load level.

422

423 *Representation of the results in the deviatoric planes*

424 A convenient representation of such complex load paths can be obtained by projecting  
425 the load components in the deviatoric plane, described by the quantity  $L =$   
426  $[H^2 + M/D^2]^{0.5}$ . This approach does not require the size and shape of the capacity surface  
427 to be assumed and proved to be efficient for the interpretation of centrifuge data from  
428 surface and buried footings (Govoni et al. 2011). In a similar way, the displacement  
429 components can be represented in the combined form  $[u/D^2 + \theta^2]^{0.5}$ .

430 The obtained load displacement curves and load responses are presented in Figure 14, for  
431 each displacement ratio applied. In order to investigate the effect of the skirt aspect ratio,  
432 the load components,  $V$  and  $L$ , are normalised by  $A\gamma'(d + D/2)$ , which proved to be a  
433 convenient normalization for the interpretation of the penetration response. The load-  
434 displacement paths exhibit very consistent curves, in terms of shape and stiffness, with a  
435 clear peak followed by hardening.

436 The experimental load paths for the two aspect ratios,  $d/D = 0.25$  and  $d/D = 0.5$ , are  
437 compared with the analytical expression of the yield surface proposed by Byrne and  
438 Houlsby (2001). The parameters were obtained from 1g tests of surface foundations in  
439 loose sand. This provides a relatively good fit to the shape of the swipe test results,  
440 particularly at high vertical loads, though the capacity is generally underestimated and  
441 some dependence on the loading mode is evident, similar to observations reported in  
442 Bienen et al. (2006). For  $u/D\theta = \infty$  and  $u/D\theta = -1.15$  (Figure 14 b and d)



443 respectively, a non-negative deviatoric vertical load is observed, as already commented  
444 on for previous plots. For displacement ratios  $u/D\theta = -0.1$  and  $u/D\theta = 1.15$  (Figure  
445 14 f and g) a transition point can be observed, with a sliding surface developing with a  
446 constant slope, independent of the skirt length and vertical load level. The effect of the  
447 skirt length is particularly evident for  $u/D\theta = -0.1$ . The increase of the yield surface  
448 with increase in aspect ratio is unconnected to the stress level. From this representation  
449 emerges more clearly the dependence of the quality of the fit on the load path.

450

451 *Description of VHM yield surface for skirted foundations in sand*

452 All experimental swipe tests results are plotted in Figure 15 in terms of  $Q/V_0$  vs  $V/V_0$ .  
453 This representation allows evaluation of the yield surface size and shape against the  
454 experimental data at one glance, rearranging Eq. 1, by combining the horizontal and  
455 moment load in the form:

$$Q = \sqrt{\left(\frac{(M/V_0)^2}{m_0^2}\right) + \left(\frac{(H/V_0)^2}{h_0}\right) - 2\alpha \frac{(M/V_0)(H/V_0)}{m_0 h_0}} \quad \text{Eq. 7}$$

456 The capacity for the aspect ratio  $d/D = 0.25$  is better captured by the fit proposed by Byrne  
457 and Houlsby (2001) than  $d/D = 0.5$ . An effect of the load path and stress level is also  
458 observed. This fitting suits best the displacement ratios  $u/D\theta = \infty$  and  $u/D\theta = -1.15$   
459 and high stress levels.

460 In order to further compare the experimental data with the available sets of parameters,  
461 the fitting obtained for Villalobos et al. (2006) is presented in Figure 16. Even if the  
462 introduction of the tension factor could capture the potential tensile capacity of the  
463 foundations, this set of parameters is not able to adequately describe the response. In  
464 comparison to the parameter set suggested by Byrne and Houlsby (2001), the size of the  
465 yield surface, in particular in the horizontal direction ( $h_0$ ), appears to be over-estimated  
466 by the parameter values provided in Villalobos et al. (2006). Further, the large negative  
467 eccentricity in the HM plane, defined by  $\alpha$ , fails to unite the experimental results.

468 The best fit of the yield surface is described by a new set of parameters, reported in Table  
469 5, with results presented in Figure 17. This is an improvement on the fitting obtained from  
470 Byrne and Houlsby (2001), and the best possible without introducing further complexity  
471 to the yield surface expression. For the design point of view, the suggested combination  
472 of yield surface parameters (Table 5) provides a conservative approximation of the  
473 capacity for a foundation with aspect ratio  $d/D = 0.5$  for some load paths (Figure 17b)  
474 whilst adequately accommodates the VHM capacity of the foundation with lower aspect  
475 ratio (Figure 17a). For the same reason of providing a conservative design approach, a  
476 tensile factor  $t_0$  was not incorporated in the yield surface formulation, as the experimental  
477 evidence is insufficient for relying on the mobilisation of tensile capacity in design.

478 At lower stresses, the experimental data indicate  $h_0$  and  $m_0$  to be larger than suggested by  
479 the overall fit. This is in line with findings by Byrne and Houlsby (2001) and Govoni et  
480 al. (2011). The centrifuge experimental data require the eccentricity parameter  $\alpha$  to be  
481 positive for the yield surface expression to provide a close fit. This contrasts with  
482 published recommendations for flat and spudcan foundations on sand but agrees with  
483 suggestions for foundations on clay. This is most probably due to the variation of soil  
484 strength over the depth that the skirted foundations mobilise the soil failure mechanism.  
485 A value of 1 for the shaping parameters  $\beta_1$  and  $\beta_2$  fits the data well overall. However, the  
486 yield surface shape shows some variation depending on the load path. Combinations  
487 dominant in horizontal loading require  $\beta_2 < \beta_1$ , i.e. a bias of the yield surface peak  
488 towards lower vertical load, whereas the converse holds for moment dominant load paths,  
489 with larger capacity available at high vertical loads than a yield surface with  $\beta_1 = \beta_2$   
490 describes, as seen in Figure 14.

491

492

### 493 **CONCLUDING REMARKS**

494 This work presents the results of centrifuge tests of skirted foundations in loose silica  
495 sand under combined VHM loading, with an emphasis on the effect of relative stress level  
496 and skirt aspect ratio on the shape and size of the yield surface. The results are compared  
497 with available previous studies on shallow skirted foundations at 1g and centrifuge tests  
498 on surface and spudcan foundations.

499

500 The findings indicate that the well-established framework of strain-hardening plasticity  
501 is relevant to skirted foundations in sand under prototype stress conditions. The  
502 experimental results indicate the level of vertical load, the skirt aspect ratio and the load  
503 combination all influence the available capacity. A simplified description of the overall  
504 yield surface size and shape is provided.

505 Comparison with results from 1g test results underline the importance of modelling at  
506 stress levels relevant to prototype conditions for capturing the vertical load response  
507 accurately. Low stress levels characterising the 1g environment lead to an  
508 underestimation of the hardening response. In contrast, comparison of combined loading  
509 tests performed in the centrifuge environment with established yield surfaces in VHM  
510 load space based on 1g tests, results in good agreement.

511

512

### 513 **ACKNOWLEDGEMENTS**

514 This work forms part of the activities of the Centre for Offshore Foundation Systems  
515 (COFS). Established in 1997 under the Australian Research Council's Special Research  
516 Centres Program. Supported as a node of the Australian Research Council's Centre of  
517 Excellence for Geotechnical Science and Engineering, and through the Fugro Chair in  
518 Geotechnics and Australian Laureate Fellowship, the Lloyd's Register Foundation Chair  
519 and Centre of Excellence in Offshore Foundations, the Shell EMI Chair in Offshore  
520 Engineering and. The work presented was performed while the first author was a visiting  
521 scholar at COFS, UWA, supported by the University of Bologna and ARC grant  
522 FL130/0005. This support is gratefully acknowledged.

523

### 524 **References**

525 Andersen, KH, Jostad, HP, Dyvik, R 2008, 'Penetration resistance of offshore skirted  
526 foundations and anchors in dense sand'., *Journal of Geotechnical and*  
527 *Geoenvironmental Engineering*, vol 134, no 1.

528 Bienen, B, Byrne, BW, Houlsby, GT & Cassidy, MJ 2006, 'Investigating six-degree-of-  
529 freedom loading of shallow foundations on sand'., *Géotechnique*, vol. 56, no. 6,  
530 pp.367–379.

531 Bienen, B, Cassidy, MJ & Gaudin, C 2009, 'Physical modelling of the push-over capacity

- 532 of a jack-up structure on sand in a geotechnical centrifuge’., *Canadian Geotechnical*  
533 *Journal*, vol. 46, pp.190–207.
- 534 Bienen, B, Gaudin, C & Cassidy, MJ 2007, ‘Centrifuge tests of shallow footing behaviour  
535 on sand under combined vertical-torsional loading’., *International Journal of*  
536 *Physical Modelling in Geotechnics*, vol. 7, no. 2, p.0.1-21.
- 537 Bolton, MD & Lau, CK 1988, ‘Scale effects arising from particle size’., *Proceeding of*  
538 *the International conference on geotechnical centrifuge modelling* , pp.127–131.
- 539 Byrne, BW 2000, *Investigations of suction caissons in dense sand*, University of Oxford.
- 540 Byrne, BW & Houlsby, GT 1999, ‘Drained Behaviour of Suction Caisson Foundations  
541 on Very Dense Sand’., *1999 Offshore Technology Conference (OTC)* , Houston, TX.
- 542 Byrne, BW & Houlsby, GT 2001, ‘Observation of footing behaviour on loose carbonate  
543 sands’., *Géotechnique*, vol. 51, no. 5, pp.463–466.
- 544 Byrne, BW & Houlsby, GT 2002, ‘Suction Caisson Foundations for Offshore Wind  
545 Turbines and Anemometer Masts’., *Wind Engineering*, vol. 26, no. 3, pp.145–155.
- 546 Cassidy, MJ 2007, ‘Experimental observations of the combined loading behaviour of  
547 circular footings on loose silica sand’., *Géotechnique*, vol. 57, no. 4, pp.397–401.
- 548 Cassidy, MJ, Martin, CM & Houlsby, GT 2004, ‘Development and application of force  
549 resultant models describing jack-up foundation behaviour’., *Marine Structures*, vol.  
550 17, no. 3, pp.165–193.
- 551 Cheng, N 2015, *Force resultant Models for Shallow Foundation Systems and Their*  
552 *Implementation in the Analysis of Soil Structure Interactions*, University of Western  
553 Australia, Perth.
- 554 Cheng, N & Cassidy, MJ 2016a, ‘Combined loading capacity of spudcan footings on  
555 loose sand’., *International Journal of Physical Modelling in Geotechnics*, vol. 16,  
556 no. 1, pp.31–44.
- 557 Cheng, N & Cassidy, MJ 2016b, ‘Development of a force–resultant model for spudcan  
558 footings on loose sand under combined loads’., *Canadian Geotechnical Journal*, vol.  
559 53, pp.2014–2029.
- 560 Christophersen, HP 1993, ‘The non-piled foundation system of the Snorre field’., *Proc.*  
561 *Offshore Site Invest. Found. Behav., Soc. Underwater tech.* , p.28: 433-447.
- 562 Foglia, A, Gottardi, G, Govoni, L & Ibsen, LB 2015, ‘Modelling the drained response of  
563 bucket foundations for offshore wind turbines under general monotonic and cyclic  
564 loading’., *Applied Ocean Research*, vol. 52, pp.80–91.
- 565 Gottardi, G & Butterfield, R 1995, ‘The displacement of a model rigid surface footing on  
566 dense sand under general planar loading’., *Soils and Foundations, The Japanese*  
567 *Geotechnical Society*, vol. 35, no. 3, pp.71–82.
- 568 Gottardi, G, Houlsby, GT & Butterfield, R 1999, ‘Plastic response of circular footings on  
569 sand under general planar loading’., *Géotechnique*, vol. 49, no. 4, pp.453–469.
- 570 Govoni, L, Gottardi, G & Gourvenec, S 2010, ‘Centrifuge modelling of circular shallow  
571 foundations on sand’., *International Journal of Physical Modelling in Geotechnics*,  
572 vol. 10, no. 2, pp.35–46.

- 573 Govoni, L, Gourvenec, S & Gottardi, G 2011, 'A centrifuge study on the effect of  
574 embedment on the drained response of shallow foundations under combined  
575 loading', *Géotechnique*, vol. 61, no. 12, pp.1055–1068.
- 576 Houlsby, GT 2016, 'Interactions in offshore foundation design', *Géotechnique*, vol. 66,  
577 no. 10, pp.791–825. Houlsby, GT & Byrne, BW 2005, 'Design procedures for  
578 installation of suction caissons in sand', *Geotechnical Engineering*, vol. 158, no. 3,  
579 pp.135–144.
- 580 Houlsby, GT, Ibsen, LB & Byrne, BW 2005, "Suction caissons for wind turbines", *Proc.*  
581 *International Symposium in Offshore Geotechnics*, pp.85-93.
- 582 Jaeger, R, DeJong, J, Boulanger, R, Low, H & Randolph, MF 2010, 'Variable penetration  
583 rate CPT in an intermediate soil', *2nd International Symposium on Cone*  
584 *Penetration Testing*.
- 585 Liu, QB & Lehane, BM 2012, 'The influence of particle shape on the (centrifuge) cone  
586 penetration test (CPT) end resistance in uniformly graded granular soils',  
587 *Géotechnique*, vol. 62, no. 11, pp.973–984.
- 588 Martin, CM 2003, 'New software for rigorous bearing capacity calculations', *Proc.*  
589 *International Conference on Foundations*, pp.581–592.
- 590 Nova, R & Montrasio, L 1991, 'Settlements of shallow foundations on sand',  
591 *G&echnique*, vol. 41, no. 2, pp.243–256.
- 592 Tan, K 1990, *Centrifuge and theoretical modelling of footings on sand*, University of  
593 Cambridge, UK.
- 594 Tjelta, TI 2015, 'The suction foundation technology', *Proceeding of the Third*  
595 *International Symposium on Frontiers in Offshore Geotechnics*, pp.85.
- 596 Villalobos Jara, FA 2006, 'Model Testing of Foundations for Offshore Wind Turbines',  
597 University of Oxford.
- 598 Zhang, Y, Bienen, B & Cassidy, M 2013, 'Development of a combined VHM loading  
599 apparatus for a geotechnical drum centrifuge', *International Journal of Physical*  
600 *Modelling in Geotechnics*, vol. Volume 13, no. 1, p.18.

601

602

603

604

605 Table 1: Summary of representative work on drained VHM capacity of shallow foundations on sand.

Reference	Foundation type	D (mm)	d/D (-)	V/A (kPa)	Dr (%)	g level	$h_0$	$m_0$	$\alpha$	$\beta_1$	$\beta_2$	$t_0$
Gottardi et al. (1999)	flat	100	0	~200	75%	1	0.1213	0.09	-0.2225	1	1	0
Byrne & Houlsby (1999), Byrne (2000)	flat	100	0	~127	95%	1	0.11	0.08	0.06	1	1	0
	caisson		0.166				0.15	0.074	-0.25			
			0.33				0.17	0.074	-0.75			
			0.66				0.13	0.09	-0.93			
Byrne & Houlsby (2001)	flat	150	0	~90	Loose (carbonate)	1	0.154	0.094	-0.25	0.82	0.82	0
Houlsby & Cassidy (2002)	flat	100	0	~200	75%	1	0.116	0.086	-0.2	0.9	0.9	0
Bienen et al. (2006)	flat	150	0	~50	5%	1	0.122	0.075	-0.112	0.76	0.76	0
Cassidy (2007)	flat	60	0	~300	45%	100	* <sup>1</sup>	*	*	*	*	0
Villalobos et al. (2009)	caisson	50.9	0.5	~300	23%	1	0.279	0.128	-0.84	0.89	0.99	0.12
			1				0.235	0.124	-0.87	0.93	0.99	0.16
Govoni et al. (2011)	flat	30,	0	~500	50%	100	0.154	0.094	-0.25	0.82	0.82	0
	buried	50	0.5				NA	NA	NA	NA	NA	0

<sup>1</sup> Fitting coefficients refers to Byrne & Houlsby (2001) and Bienen et al. (2006)

Combined loading capacity of skirted circular foundations in loose sand  
 Fiumana, Bienen, Govoni, Gourvenec, Cassidy & Gottardi

			1				NA	NA	NA	NA	NA	$v_t^2=0.085$
Cheng & Cassidy (2016)	spudcan	60	0	~300	35%	100	0.113	0.096	-0.248	0.71	0.99	0
	skirted		0.133	~500	35%		0.21	0.097	-0.51	0.77	0.96	0
					90%		0.37	0.15	0.5	0.81	0.99	0
This study	skirted	50	0.25	~100 - 500	30%	100						3
			0.5									

606

<sup>2</sup> parameter which accounts for a non-linear expansion of the yield surface with the embedment of the foundation and used to fit the data close to the origin (Govoni et al. 2011)

607 Table 2: Material properties of sand used in centrifuge tests (Liu & Lehane 2012).

<b>Property</b>	<b>Value</b>
$G_s$	2.650
$D_{50}$ (mm)	0.150
$e_{min}$	0.449
$e_{max}$	0.747
$\phi_{cv}$ (°)	31

608



609

610 Table 3: Summary of swipe tests (in prototype dimensions).

Type of tests	Test name	d/D	Target		Measured			Swipe parameters			
			V/A (kPa)	w <sub>0</sub> (m)	V <sub>0</sub> (MN)	w <sub>0</sub> (m)	w <sub>0</sub> /D (-)	u/Dθ (rad <sup>-1</sup> )	u (m)	θ (°)	
Vertical penetration	VP_0.25	0.25	-	-		-	-	-	-	-	
	VP_0.5	0.5	-	-		-	-	-	-	-	
Load-unload	LU_0.25	0.25	-	-		-	-	-	-	-	
	LU_0.5	0.5	-	-							
SWIPE TESTS	ARRANGEMENTS FOR JACKET STRUCTURES	SW1	0.25	~500	~1.7	<b>11.85</b>	1.92	0.38	∞	0.9	0
		SW2	0.25	~500	~1.7	<b>11.6</b>	1.91	0.38	-1.15	0.9	-9
		SW3	0.25	~500	~1.7	<b>9.14</b>	1.84	0.37	-0.1	0.09	-9
		SW4	0.25	~500	~1.7	<b>10.65</b>	1.84	0.37	1.15	-0.9	-9
		SW9	0.5	~500	~2.8	<b>11.07</b>	2.91	0.58	∞	0.9	0
		SW10	0.5	~500	~2.8	<b>9.81</b>	2.91	0.58	-1.15	0.9	-9
		SW11	0.5	~500	~2.8	<b>12.16</b>	2.96	0.59	-0.1	0.09	-9
		SW12	0.5	~500	~2.8	<b>9.61</b>	2.90	0.58	1.15	-0.9	-9
	MONOPOD FOR WIND TUBINE	SW5	0.25	~100	~1.3	<b>2.89</b>	1.31	0.26	∞	0.9	0
		SW6	0.25	~100	~1.3	<b>2.30</b>	1.31	0.26	-1.15	0.9	-9
		SW7	0.25	~100	~1.3	<b>4.1</b>	1.34	0.27	-0.1	0.09	-9
		SW8	0.25	~100	~1.3	<b>2.84</b>	1.32	0.26	1.15	-0.9	-9
		SW13	0.25	~100	~2.5	<b>4.87</b>	2.66	0.53	∞	0.9	0
		SW14	0.25	~100	~2.5	<b>5.83</b>	2.70	0.54	-1.15	0.9	-9
		SW15	0.25	~100	~2.5	<b>5.5</b>	2.69	0.53	-0.1	0.09	-9
		SW16	0.25	~100	~2.5	<b>3.83</b>	2.67	0.53	1.15	-0.9	-9

611

612

613

614 Table 4: Details of vertical penetration tests (after Villalobos 2006)

Test name	d/D	Dr (%)	w <sub>0</sub> /D	V <sub>0</sub> /A (kPa)
FV62	0.26	26	0.25	4.00
FV21	0.26	40	0.26	3.00
FV63	0.51	26	0.51	6.00
FV22	0.51	40	0.49	5.00

615

616

617 Table 5: Yield surface parameters (overall fit) for Eq. 1

Parameters	Value	Description
h <sub>0</sub>	0.16	Size in the horizontal plane
m <sub>0</sub>	0.13	Size in the moment plane
α	0.6	Eccentricity
β <sub>1</sub>	1	Shaping parameter
β <sub>2</sub>	1	Shaping parameter

618

619

620

621 **LIST OF FIGURES:**

622 Figure 1: Offshore energy infrastructure supported by skirted foundations as a) monopod,  
623 b and d) jacket with multiple foundations, c) jack-up with typically three foundations.

624 Figure 2: Schematic representations of the yield surface for skirted foundations on sand  
625 in drained conditions based on 1g experiments: a) shape and size governed by the  
626 mobilised stress level and  $M/(HD)$  ratio and b) allowance for horizontal and moment  
627 capacity in the tensile range of vertical load.

628 Figure 3: Centrifuge set-up, foundation model and sign convention.

629 Figure 4: Movements of the VHM actuator that result in rotation about the reference point  
630 (RP) after Zhang et al. (2013).

631 Figure 5: Characterization of sand sample from miniature CPT, in terms of a) measured  
632 and net cone resistance,  $q_c$  and  $q_{net}$  and b) relative density  $D_r$ .

633 Figure 6: Vertical load-penetration curves, a) in prototype dimensions, b) normalised.

634 Figure 7: Vertical unloading stiffness.

635 Figure 8: Normalised load-penetration curves.

636 Figure 9: Swipe test results for a test dominated by moment.

637 Figure 10: Swipe test results for a test dominated by horizontal load.

638 Figure 11: Results of all swipe tests in the a) VH, b) VM/D planes.

639 Figure 12: Results of all swipe tests in the a)  $H/V_0$  vs  $V/V_0$ , b)  $M/DV_0$  vs  $V/V_0$  planes.

640 Figure 13: Result of all swipe tests in the  $M/D$  vs  $H$  plane in prototype units for a)  $d/D =$   
641  $0.25$  and b)  $d/D = 0.5$ .

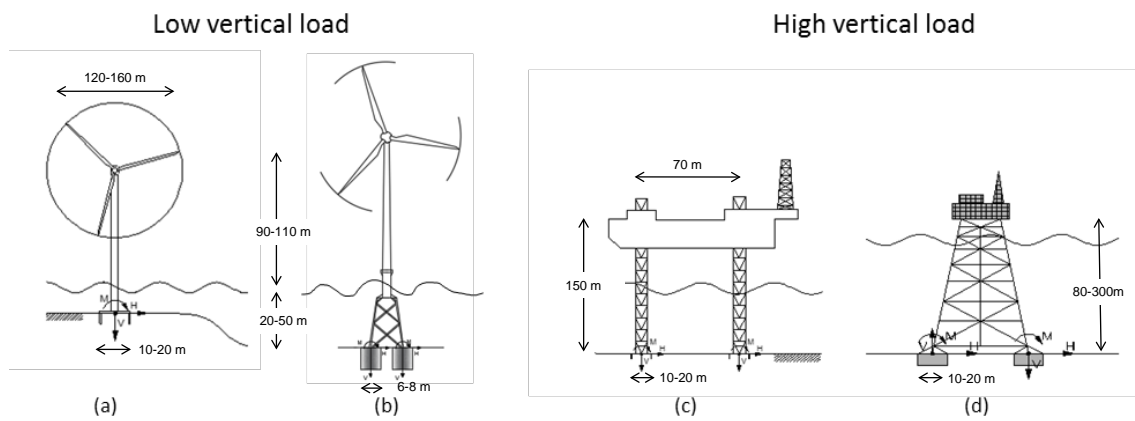
642 Figure 14: Result of all swipe tests in the a)  $[(u/D)^2 + 0.2]^{0.5}$  vs  $L/A \gamma'(d+D/2)$ , b)  $V/$   
643  $A \gamma'(d+D/2) : L/A \gamma'(d+D/2)$  plane, compared with eq. 1 for surface foundations (Byrne  
644 & Houlsby 2001).

645

646 Figure 15: Experimental results with VHM yield surface, overall fit for Houlsby and  
647 Byrne parameters (2001), a)  $d/D=0.25$ , b)  $d/D=0.5$ .

648 Figure 16: Experimental results with VHM yield surface, overall fit for Villalobos  
649 parameters (2006), a)  $d/D=0.25$ , b)  $d/D=0.5$ .

650 Figure 17: Experimental results with VHM yield surface (overall fit), a)  $d/D=0.25$ , b)  
651  $d/D=0.5$ .



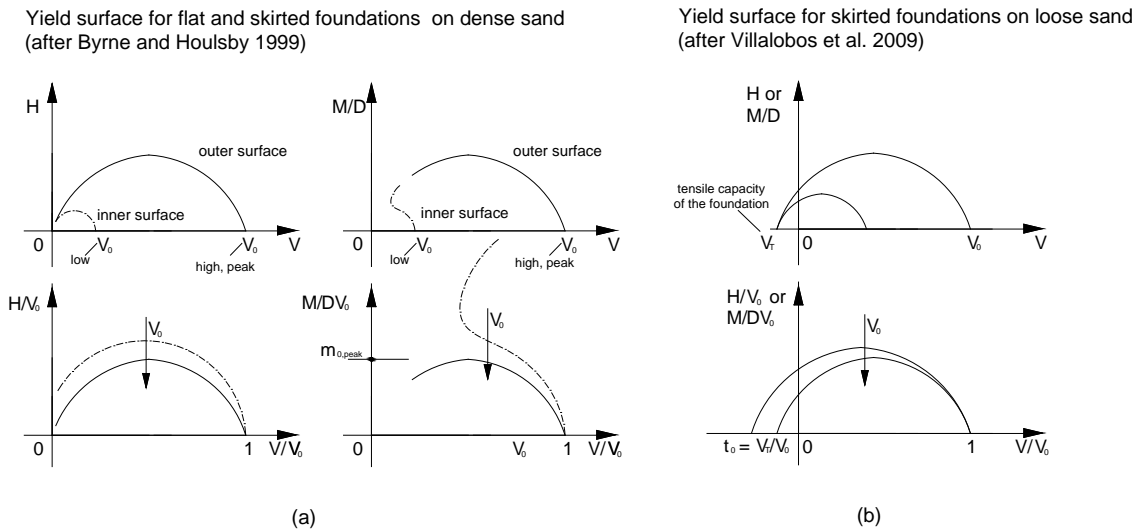
652

653

654

Figure 1: Offshore energy infrastructure supported by skirted foundations as a) monopod, b and d) jacket with multiple foundations, c) jack-up with typically three foundation.

655



656

657

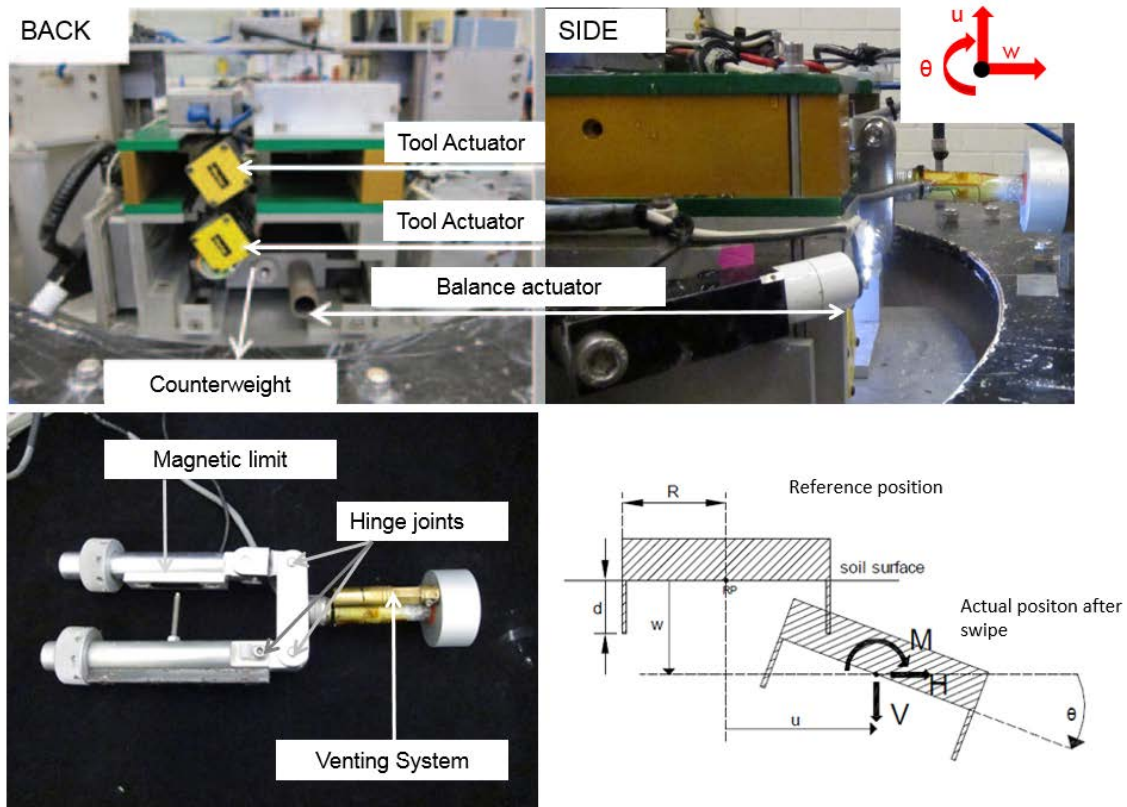
658

659

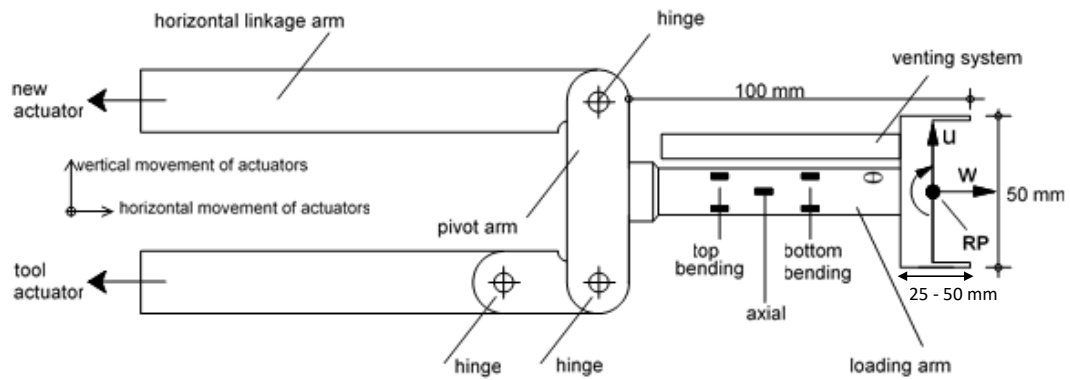
660

Figure 2: Schematic representations of the yield surface for skirted foundations on sand in drained conditions based on 1g experiments: a) shape and size governed by the mobilised stress level and  $M/(HD)$  ratio and b) allowance for horizontal and moment capacity in the tensile range of vertical load.

661



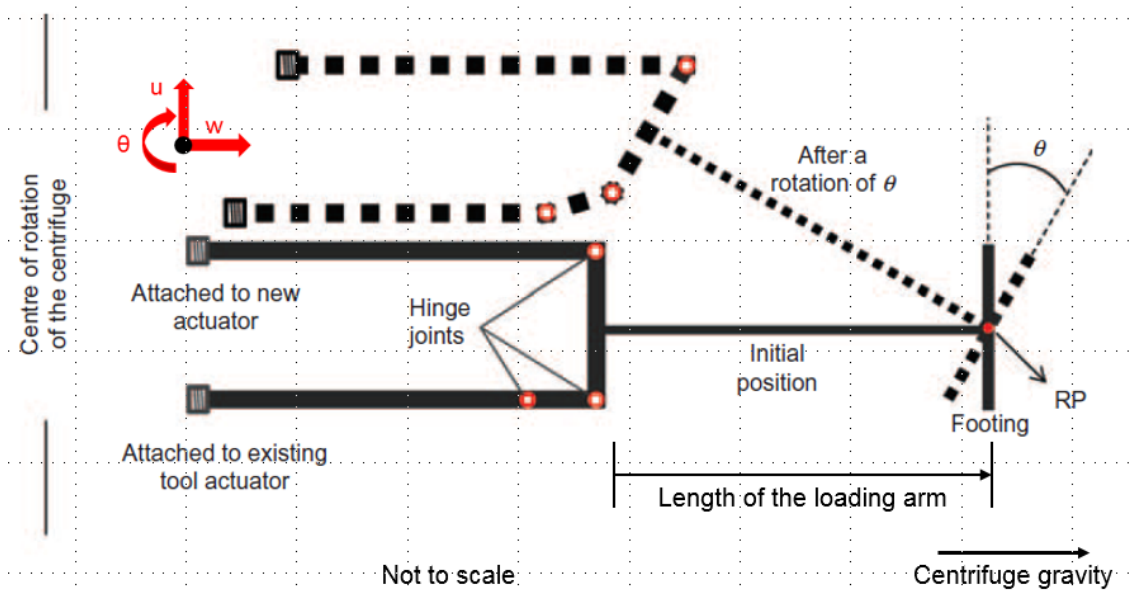
662



663

664 Figure 3: Centrifuge set-up, foundation model and sign convention.

665



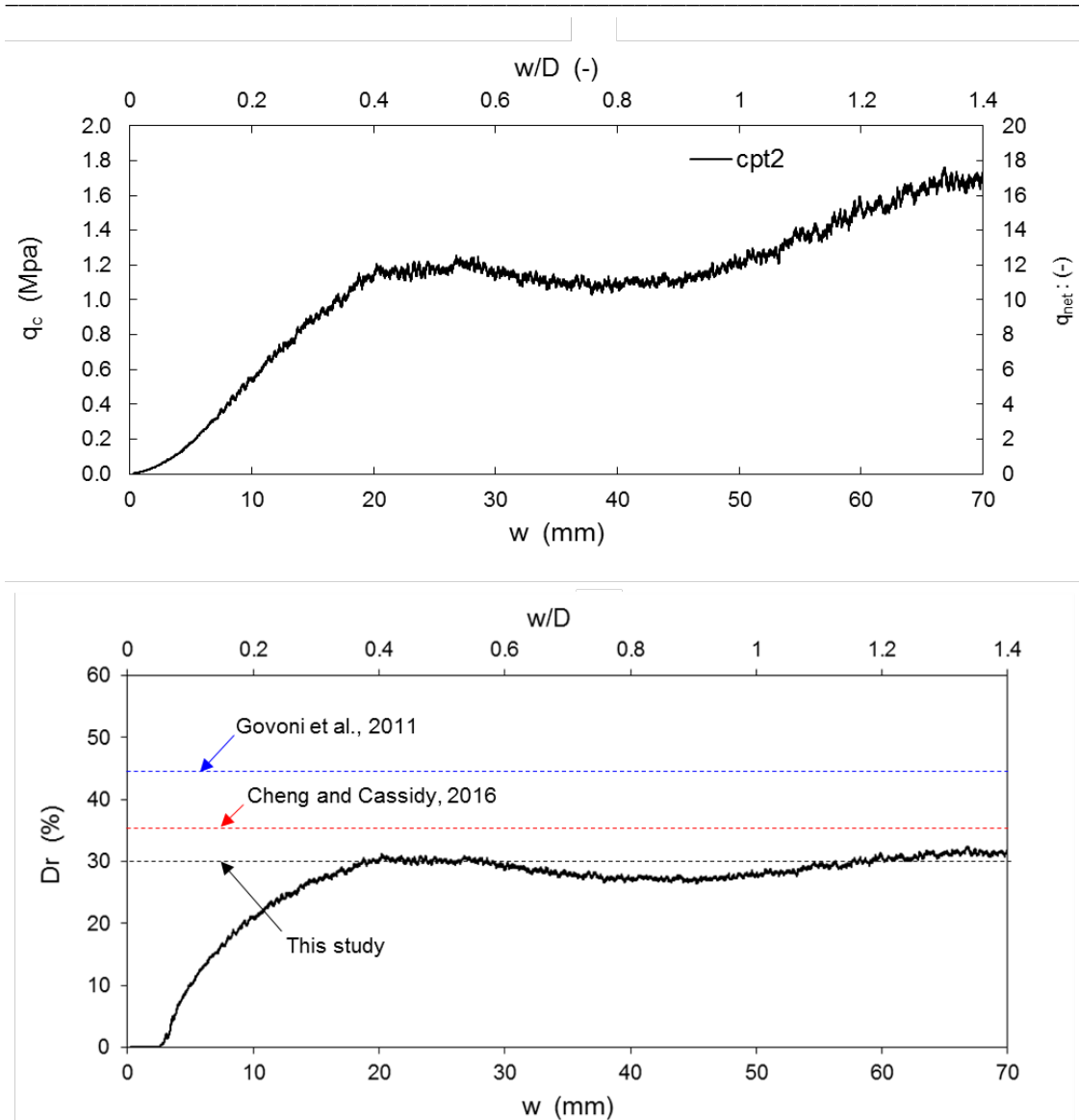
666

667 Figure 4: Movements of the VHM actuator that result in rotation about the reference point

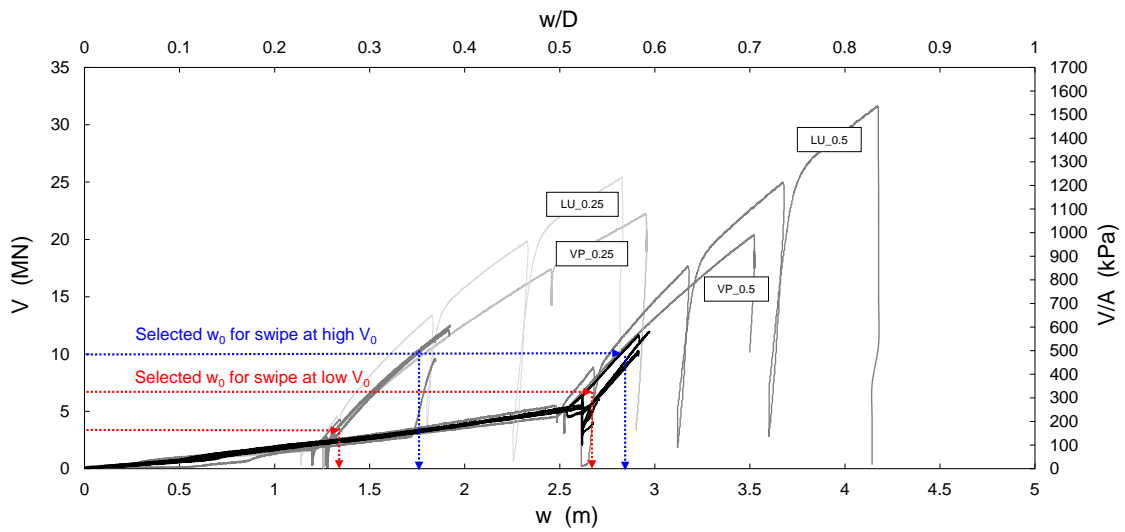
668

(RP) after Zhang et al. (2013).



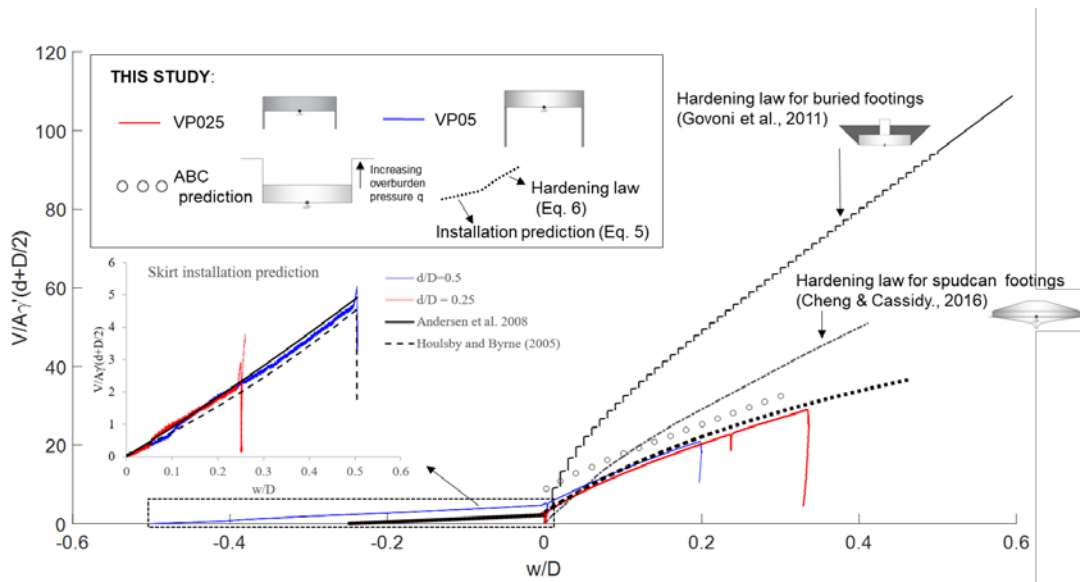


669  
670 Figure 5 Characterization of sand sample from miniature CPT, in terms of a) measured  
671 and net cone resistance,  $q_c$  and  $q_{net}$  and b) relative density  $D_r$ .



672  
 673  
 674

(a)

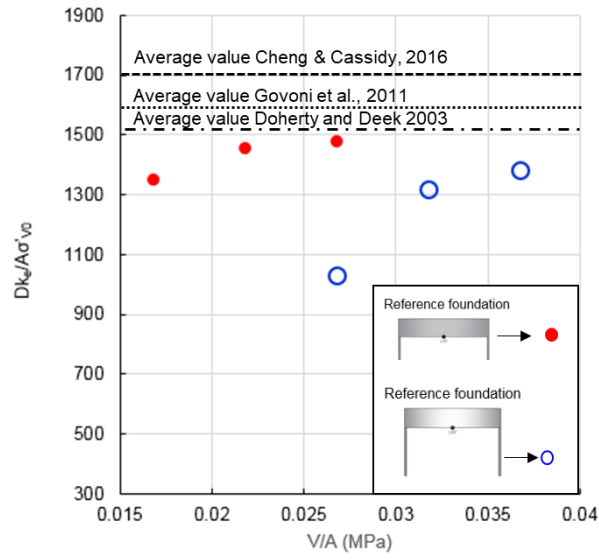


675  
 676

(b)

677 Figure 6: Vertical load-penetration curves, a) in prototype dimensions, b) normalised.

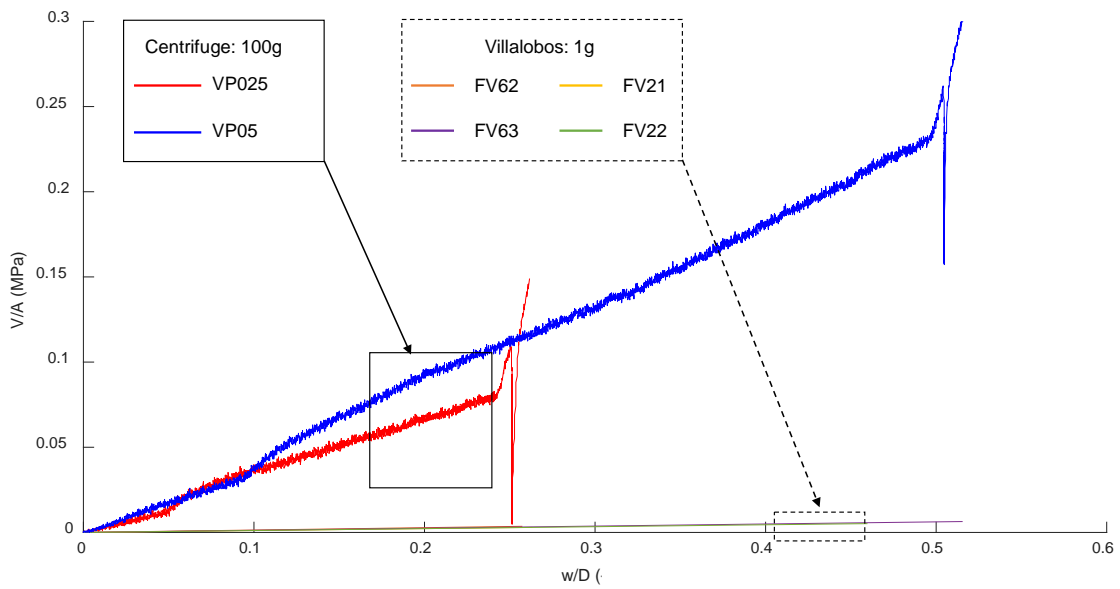
678



679

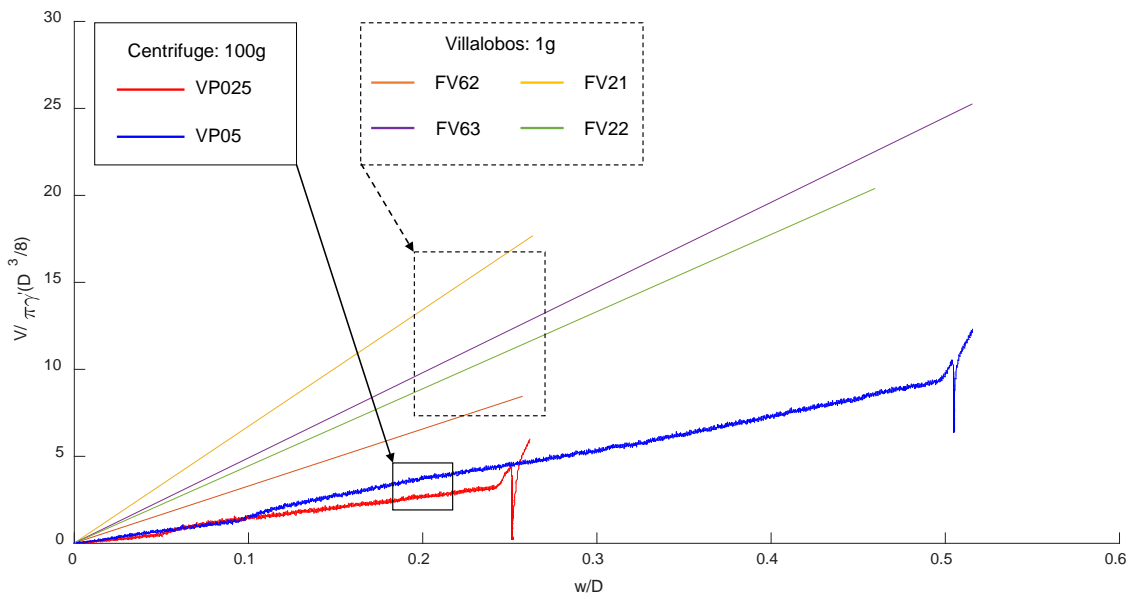
680 Figure 7: Vertical unloading stiffness.

681  
682



683  
684

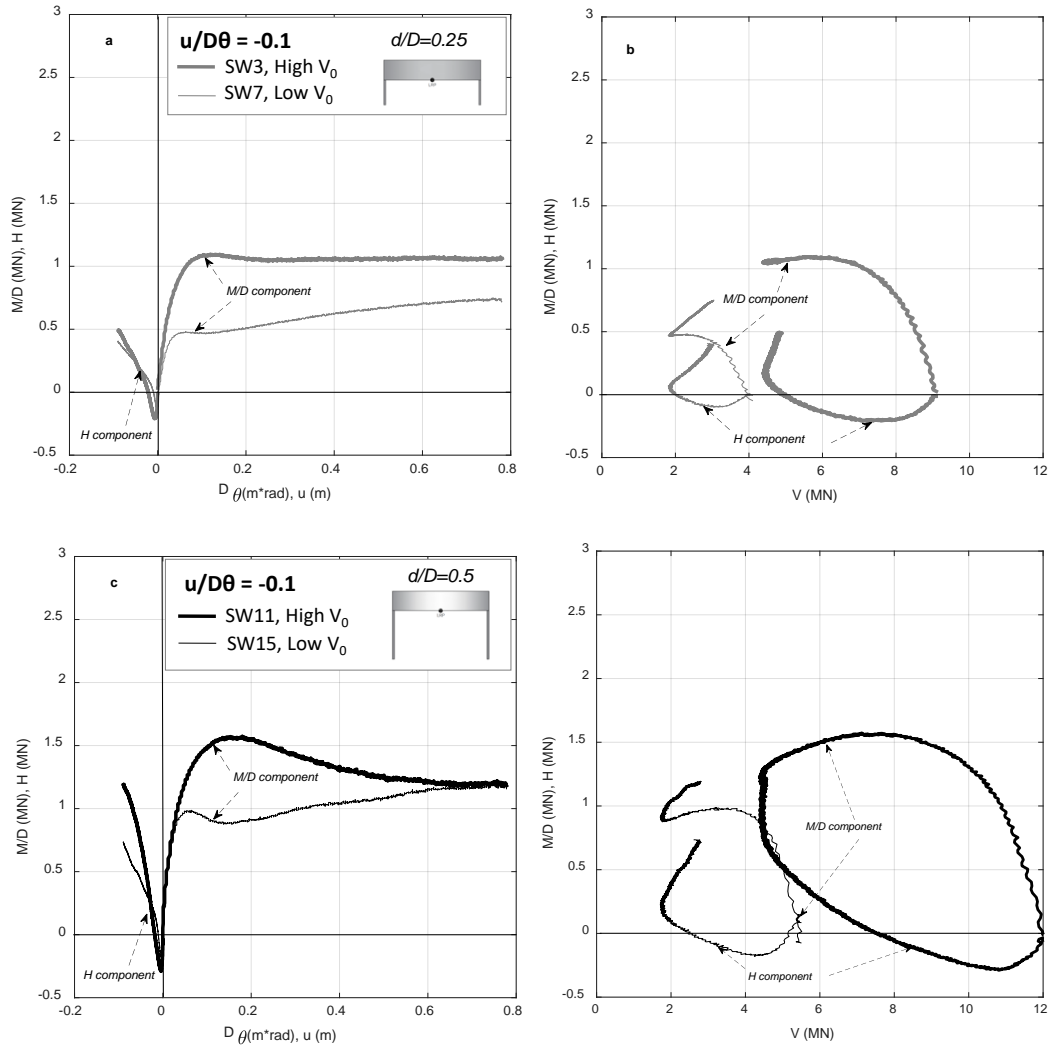
(a)



685  
686

(b)

687 Figure 8: Normalised load-penetration curves.



688 Figure 9: Swipe test results for a test dominated by moment.

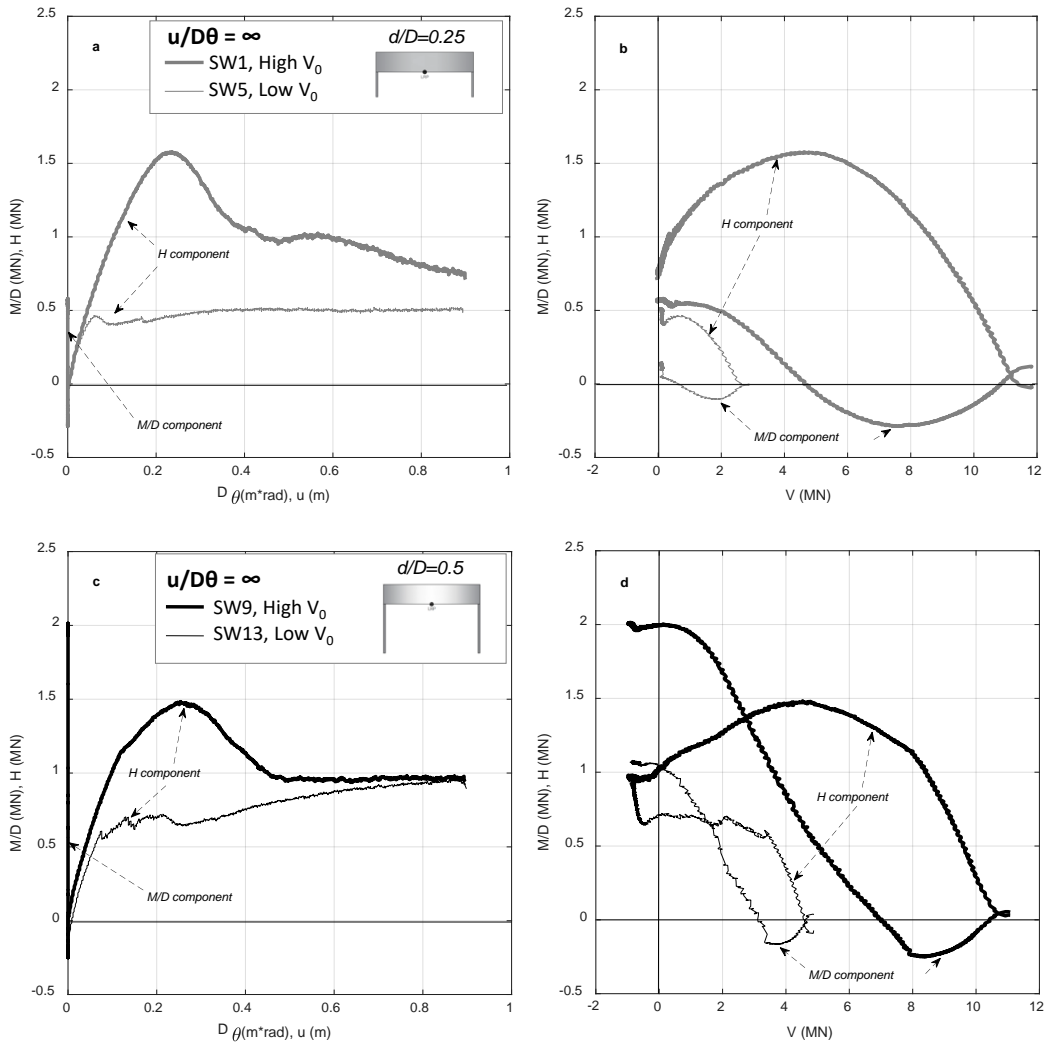
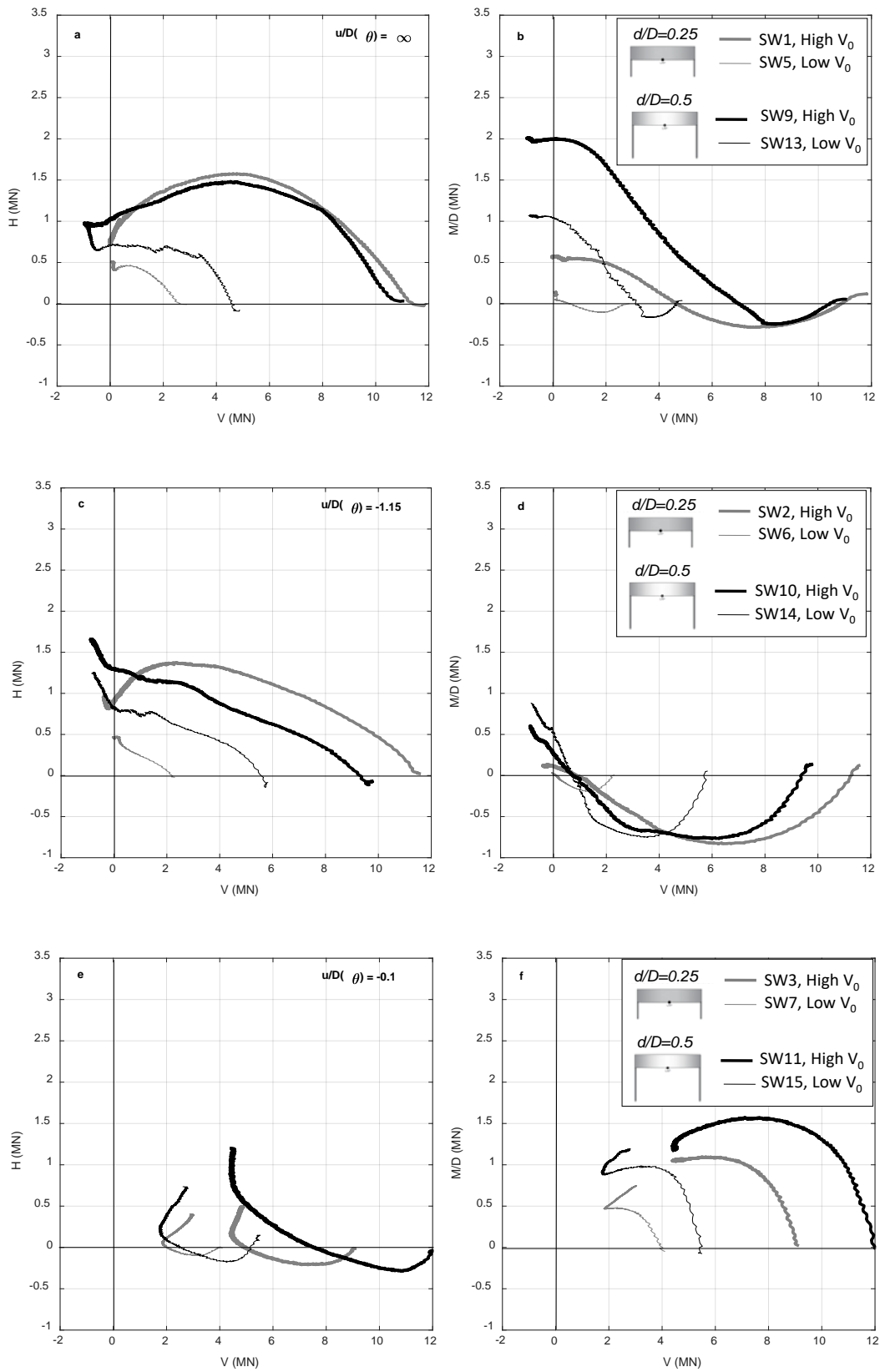


Figure 10: Swipec test results for a test dominated by horizontal load.



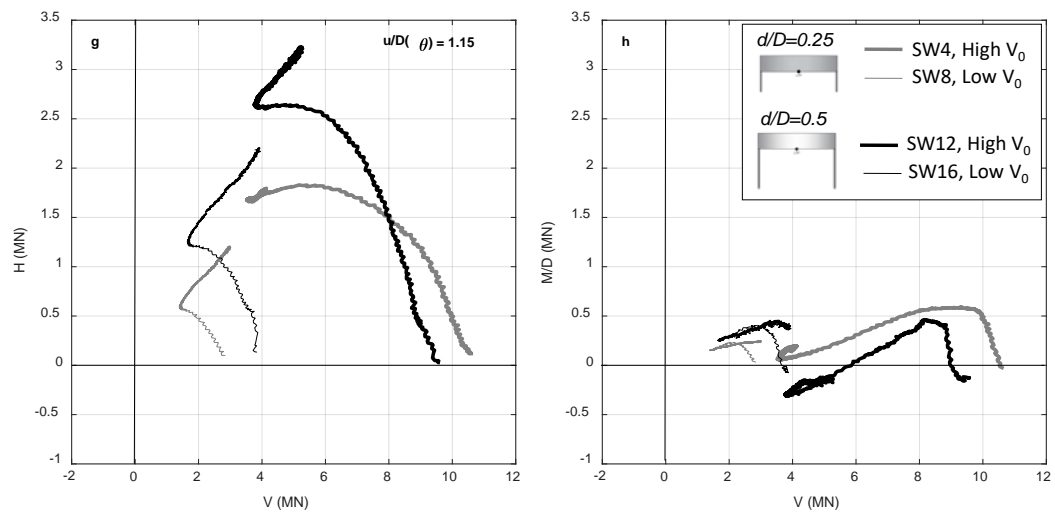
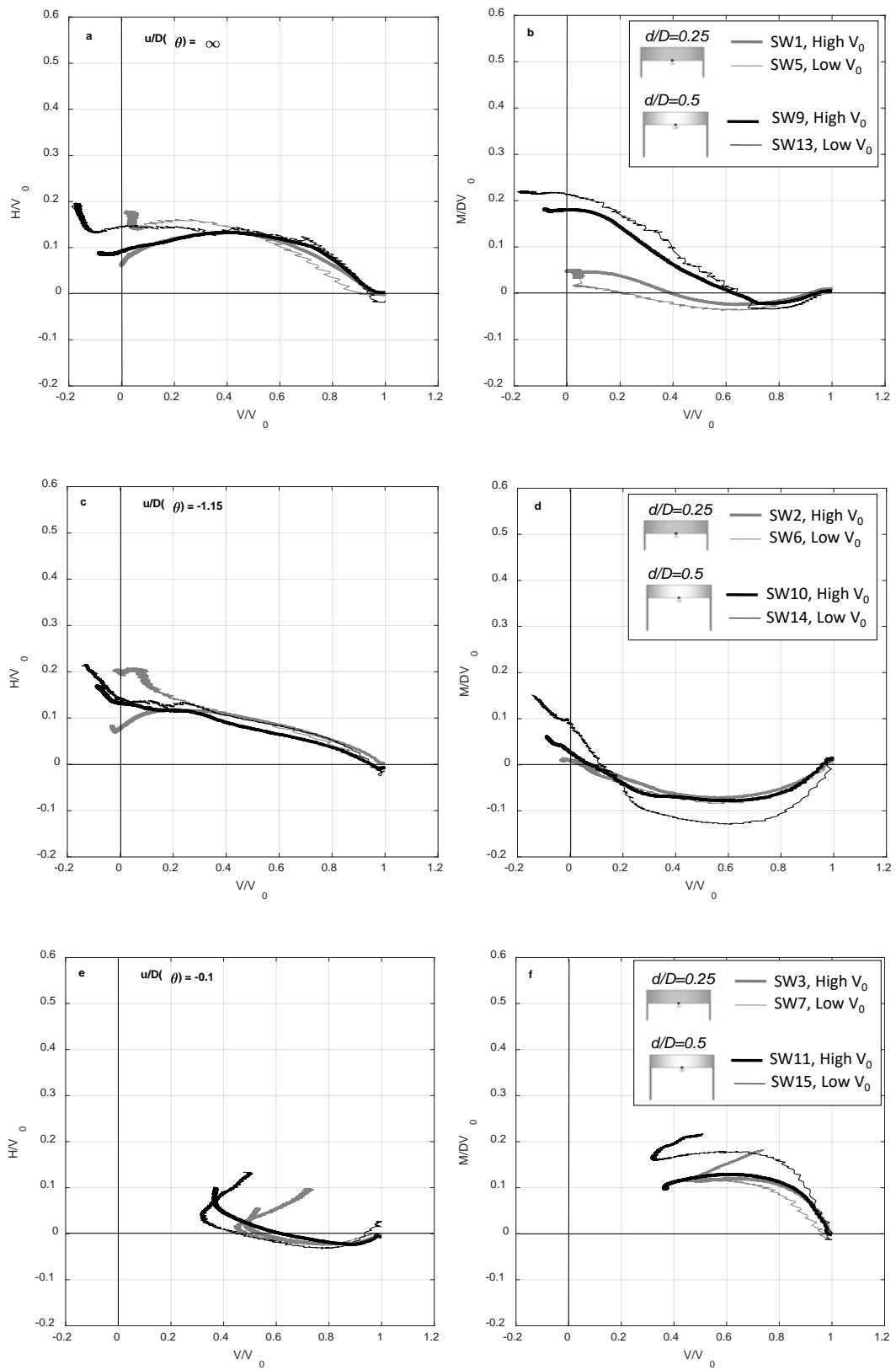


Figure 11: Results of all swipe tests in the a) VH, b) VM/D planes.

690





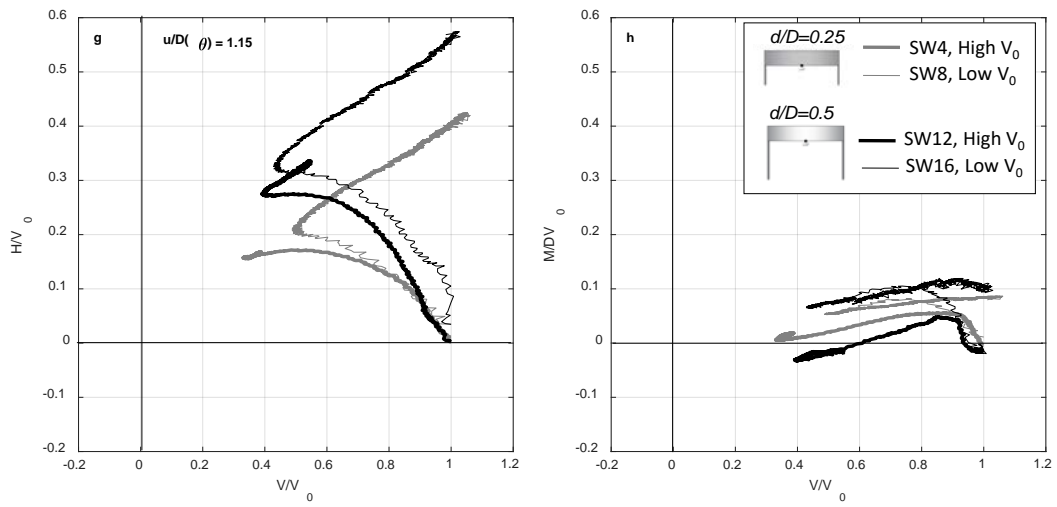
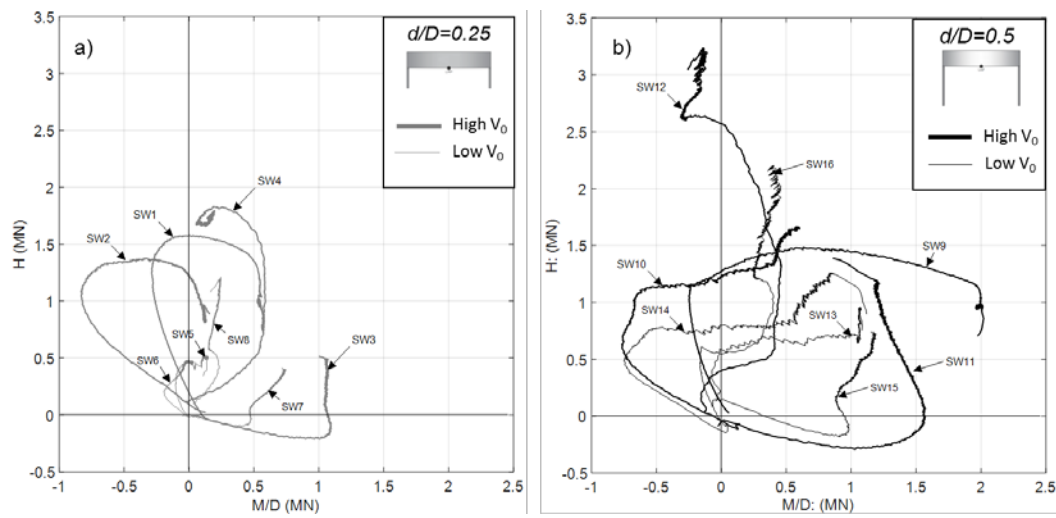
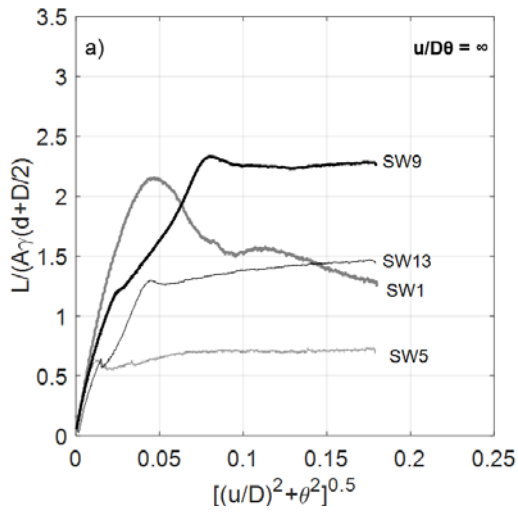


Figure 12: Results of all swipe tests in the a)  $H/V_0$  vs  $V/V_0$ , b)  $M/DV_0$  vs  $V/V_0$  planes.

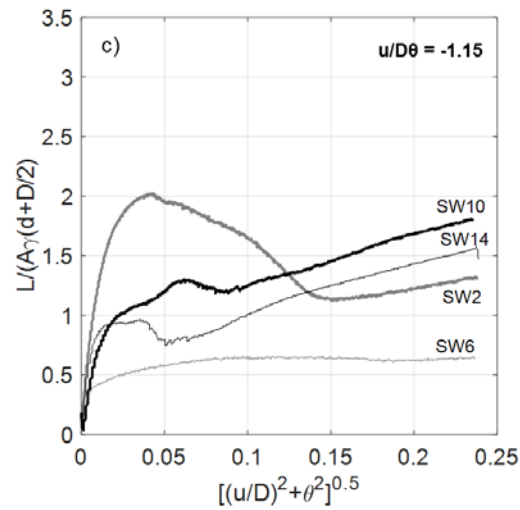
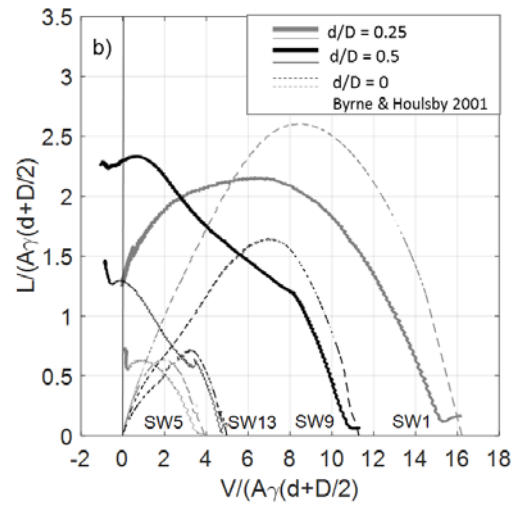


692

693 Figure 13: Result of all swipe tests in the  $M/D$  vs  $H$  plane in prototype units for a)  $d/D =$   
694  $0.25$  and b)  $d/D = 0.5$ .

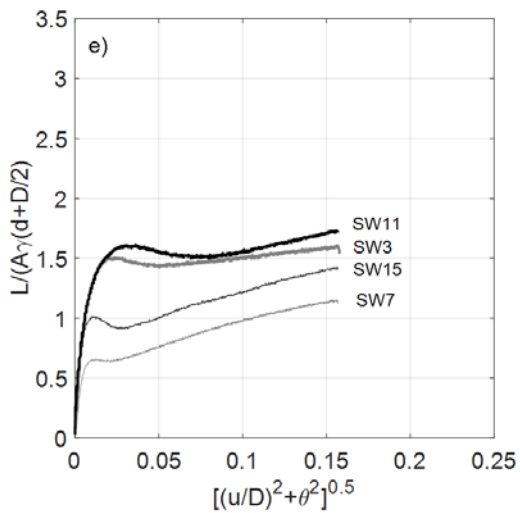
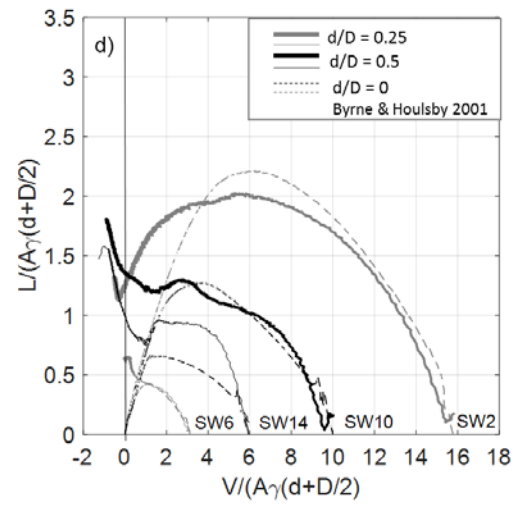


695

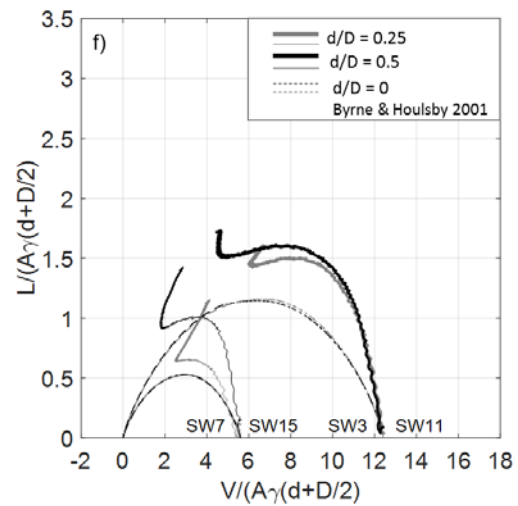


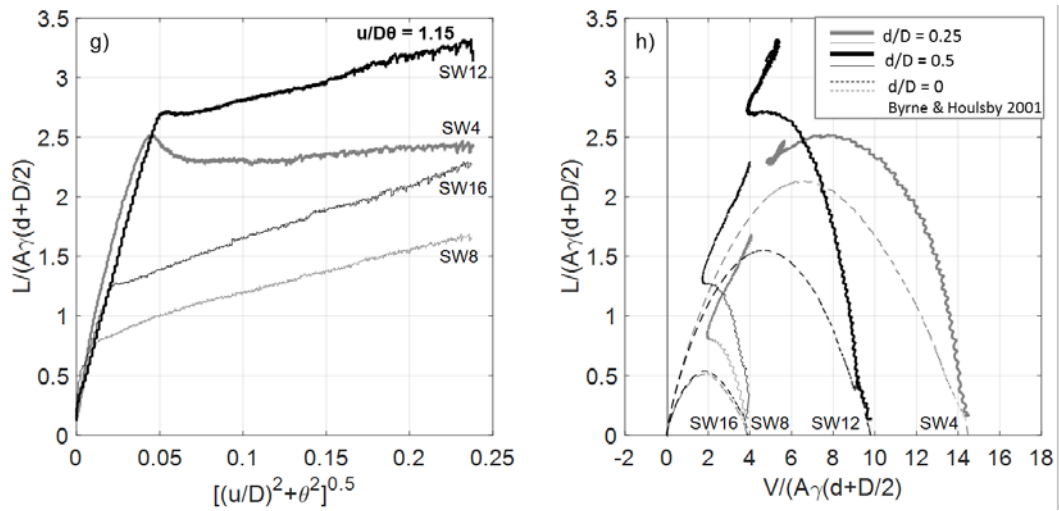
696

697



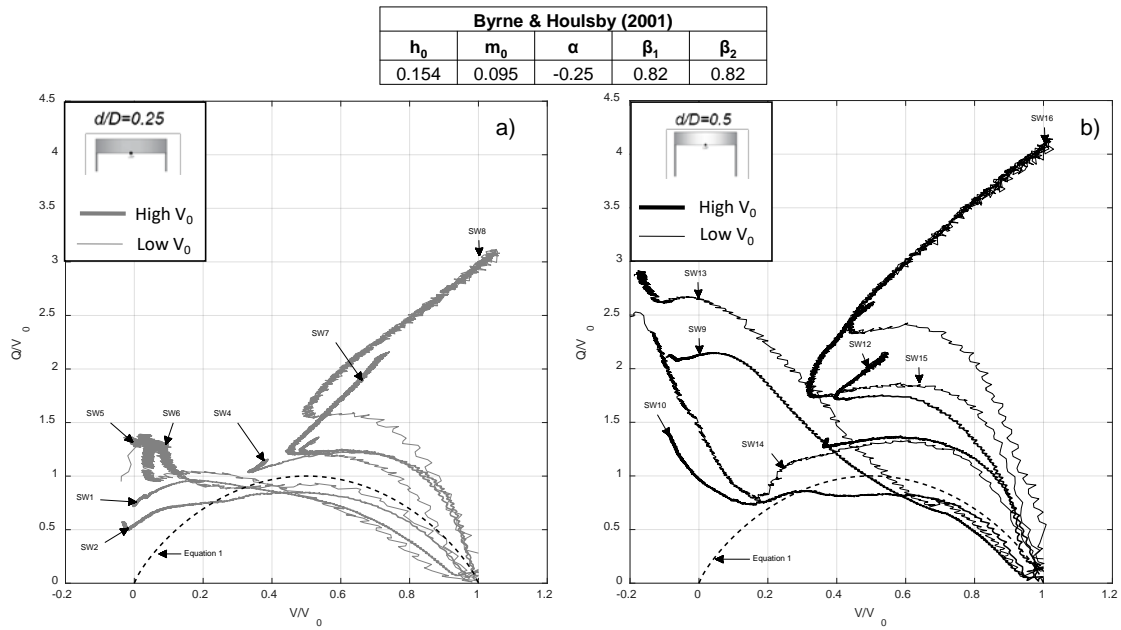
698





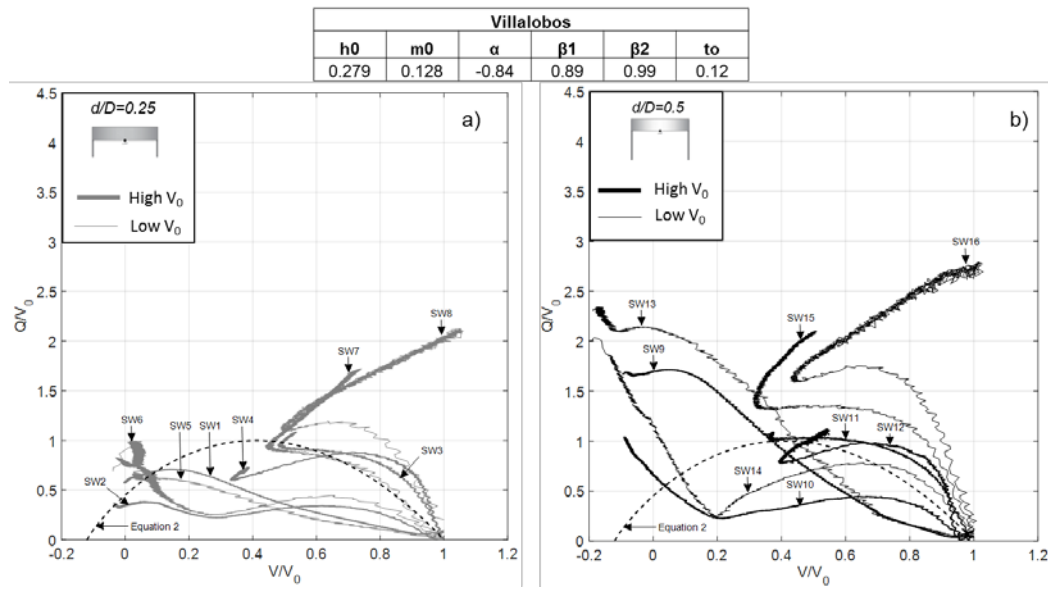
699

700 Figure 14: Result of all swipec tests in the a)  $[(u/D)^2 + \theta^2]^{0.5}$  vs  $L/A \gamma'(d+D/2)$ , b)  $V/$   
 701  $A \gamma'(d+D/2) : L/A \gamma'(d+D/2)$  plane, compared with eq. 1 for surface foundations (Byrne  
 702 & Houlsby 2001).



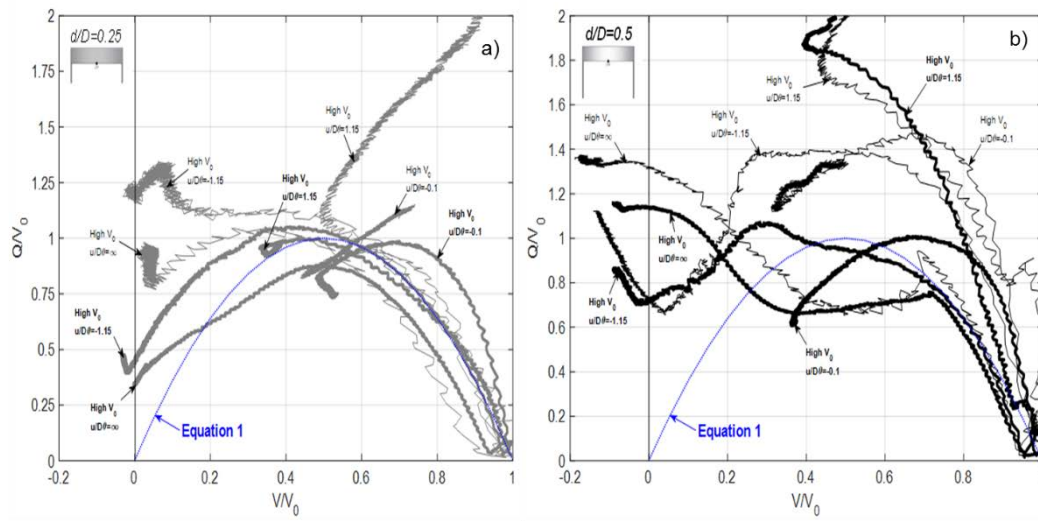
703

704 Figure 15: Experimental results with VHM yield surface, overall fit for Byrne and  
 705 Houlsby parameters (2001), a)  $d/D=0.25$ , b)  $d/D=0.5$ .



706

707 Figure 16: Experimental results with VHM yield surface, overall fit for Villalobos  
 708 parameters (2006)), a)  $d/D=0.25$ , b)  $d/D=0.5$ .



709  
710 Figure 17: Experimental results with VHM yield surface (overall fit), a)  $d/D = 0.25$ , b)  
711  $d/D = 0.5$ .

712

713

714

715

716